# Flow Induced Vibration Harvest

## Broaden the range of efficient harvesting

Jim Kok

Master of Science Thesis

TU Delft Delft University of Technology

Delft Center for Systems and Control

# Flow Induced Vibration Harvest

## Broaden the range of efficient harvesting

Master of Science Thesis

For the degree of Master of Science in Mechanical Engineering at Delft University of Technology

Jim Kok

May 17, 2017

Faculty of Mechanical, Maritime and Materials Engineering (3mE) · Delft University of Technology


# Abstract

This thesis studies ways of broadening the range of a piezoelectric flow induced vibration harvester. The proposed device consists of a flap connected with a hinge to a spring. Existing harvesters are designed to replace or charge batteries for low power systems in the range of milliwatts. These systems produce low amounts of power, but for low flow speeds. The objective of this thesis is to increase the range of efficient harvesting. To achieve such a harvester, the coupling between the spring dynamics and aerodynamics will be studied.

Considered methods for changing the dynamics of the spring are stiffness and length modifications. Besides changing the aerodynamics of the wing will also be considered as a solution. Linear state space models are derived and validated with experimental tests. After derivation of the models, changes in aerodynamics will not been seen as a feasible solution because of the required power transfer across the hinge. Despite stiffeners can contribute to the efficiency of a harvester by changes in the mode shape. Additional stiffness resulted in lower eigenfrequency changes than expected. Only the changes in length seem to have a significant influence on the range of harvesting.

# Contents

# Acknowledgements

I would like to thank my supervisor Dr.Ir. J.W. van Wingerden and Mr. C.J. Slinkman in particular for the support they gave me last year. It was J.W. van Wingerden who introduced me to the field of flow induced vibrations. He gave me the opportunity to investigate and design a flow induced vibration harvester. Partly due to the assistance of the dedicated staff member C.J. Slinkman a successful harvester has been manufactured. However, during my thesis I received support from a lot of friends as well. To avoid a long story with many names I would like to thank you all. You know what you have done for me and I am very grateful for that.

Delft, University of Technology — Jim Kok
May 17, 2017

*To my family and friends*

# Chapter 1

# Introduction

Fossil Fuels provide roughly 85% of the worldwide energy consumption [1]. Environmental concerns and declining reserves require the energy sector to get more sustainable. Renewable energy seems to be a promising solution [2, 3, 4]. A disadvantage of most renewable sources is its variability. Besides variability, the potential of renewable sources is location dependent. Often, locations with high potential are located far from urban areas. To overcome the disadvantages there is a need of reconfiguration of the existing grids [3]. Installing energy harvesters in urban areas will be beneficial to reduce the electricity transfer. Besides lowering electricity transfer, mounting energy harvesters on existing structures could be an advantage of harvesting in urban areas. However, most traditional renewable energy harvesting methods are not suitable for urban areas. Leading to the investigation of innovative methods for harvesting energy.

## 1-1 Introduction to flow induced vibration energy harvesting

This thesis will focus on wind energy as a potential energy source in urban areas. Mainly because of cost efficiency and their need of large areas, traditional turbines will not be suitable for urban areas [5, 6]. Even experiments with scaled down urban-based wind turbines have failed. Mainly because of neighbours who complain about noise and safety [6]. Furthermore, undesired vibrations and cost-effectiveness make the new turbine designs unsuccesfull. The disadvantages of traditional harvesting methods led to the investigation of novel energy extracting methods, including the flow induced vibrations energy harvesters [6].

In the past flow induced vibrations were suppressed and reduced to a minimum to prevent structures from failure by fatigue. Several years ago, the potential of flow induced vibrations for the use of energy harvesting have been investigated. This resulted in several concepts able to approach or exceed the efficiency of traditional comparable sized turbines [7]. Flow induced vibration harvesters proposed in current literature replace or charge batteries of small electronic devices. These devices only use power in the range of milliwatts. This leads to designs capable of harvesting low amounts of power for even very low wind speeds [6]. In this

thesis, the aim is to investigate the possibility of an energy harvester capable of harvesting significant amounts of power, for a wide range of flow velocities.

Researchers from different fields of expertise have investigated flow induced vibration, all using their own terminology. To prevent confusion the basic framework of Naudascher and Rockwell [8] is used. In this framework flow induced vibrations are divided into three groups:

1. Extraneously Induced Excitation, by fluctuations in the fluid flow (EIE)
2. Instability Induced Excitation, by fluctuations induced by the structure (IIE)
3. Movement Induced Excitation, by the movement of the structure (MIE)

Figure 1-1 shows a typical response of all excitation forms.

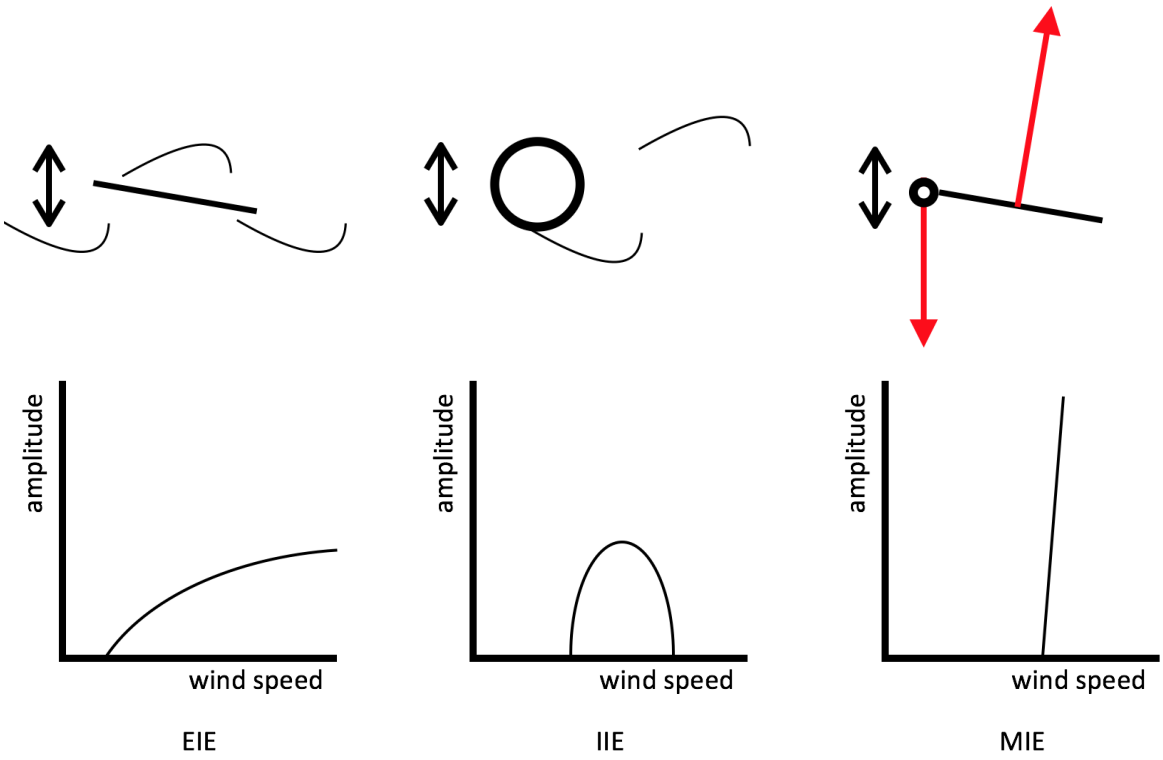


**Figure 1-1:** Typical response for the different excitation forms. [9]

Vortex shedding of a structure is an example of an IIE. The IIE differs from EIE, because EIE is caused by upstream structures and already present in the flow. An MIE is induced by the coupling between the movement and lift force. This coupling can be divided into two categories: one and two degrees of freedom MIE. One degree of freedom MIE consist of a one degree of freedom movement. Where the change in the lift force is induced by the relative velocity of the flow around the structure. The relative velocity is the resulting movement of the fluid flow and movement of the structure. A two degree of freedom system is free to move in both transversal and rotational direction. For a two degree of freedom MIE the instability is induced by the coupling between both degrees of freedom.

Especially for low wind speeds EIE is a suitable excitation form. However, instead of a static structure also upstream harvesters introduce an EIE. Wake effects of upstream MIE harvesters can increase the power production by 20% [10]. Comparable results were found for IIE harvesters [6]. This makes an EIE suitable for the enhancement of a flow induced energy harvester.

For the excitation of the harvester a choice should be made between an IIE or an MIE. Where the IIE results a limited response the response of an MIE is much larger. For the purpose of energy harvesting the larger response is desirable. However, an MIE will be induced for high flow speeds compared to an IIE. To lower the cut-in velocity of excitation the weight distribution of the harvester is an important design tool [11].

## 1-2 State-of-the-art flow induced vibration energy harvesters

McCarthy reviews a great number of flow induced energy harvesters designed in the past years [6]. He concluded that the lack of a standardisation method results in difficulties for comparison. However, MIE seems most promising when the different designs are compared on efficiency [12, 13]. Figure 1-2 compares the efficiency of scaled down urban based wind turbines and oscillating flow induced vibration harvesters [12]. Electromagnetic turbines and some of the MIE have comparable efficiencies for low flow speeds. For increasing wind speeds the efficiency of the MIE rapidly decreases. These first designs of the MIE harvesters are designed to harvest low amounts of energy for a wide range of flow velocities. Instead, a harvester design which adds maximum damping for a system with a collocated eigenfrequency and excitation frequency.

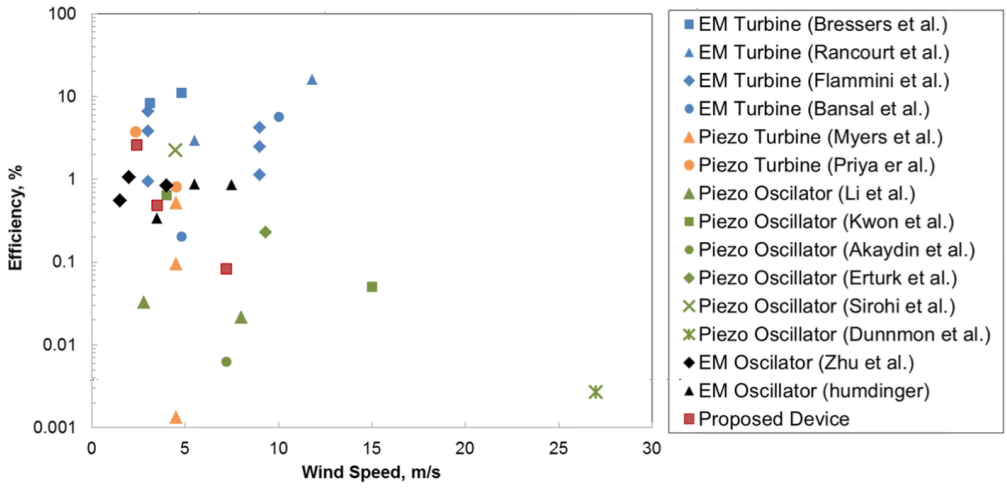


**Figure 1-2:** Effiency of scaled down turbines compared to oscillating flow induced vibration harvesters. Where the harvester designed by Bryant and Garcia (Proposed Device) is an MIE like the harvester used in this thesis. [12]

For performance enhancement stacking is one of the most applied methods, but also stiffness changes have been used. The advantage of stacking is the simplicity. Upstream harvesters produce an EIE on downstream harvesters. Dependent on the spacing the EIE increases the power output. For optimal performance the spacing between harvesters should be kept minimum, independent of the flow speed [10]. Methods used to change the stiffness of the harvester were non-linear spring and stiffeners. Both methods have proven to be effective ways to influence the harvester's performance [13, 14]. By changing the stiffness, the eigenfrequendy of the harvester is changed. This results in an increase of the operational bandwidth. Besides changing the eigenfrequency, stiffeners also change the mode shape of the harvester. Stiffeners on the spring will result in the same amount of deflection in the piezoelectric sheet, but a lower tip deflection. This will result in an increase of the harvester's efficiency.

In this thesis, the application of active control for performance enhancement is investigated. Active control can be used to optimise the harvester's dynamics dependent on the flow speed. In [13] the change in eigenfrequency of the harvester results in oscillations for different flow speeds. Potentially widening the range of flow speed and an increase in the operational envelope. Besides a large operational envelope, also harvested power should be considered for an enhanced harvester design. Extracting more energy of the system means increasing the damping of the system. To achieve such a controller, a more in depth study on the modelling of MIE will be required. It remains to be seen if lumped parameter models used in current literature will be suitable. Furthermore, a way of changing the stiffness and damping should be investigated. With the goal to show the feasibility of an effective flow induced energy harvester for a broad range of flow speeds.

## 1-3 Contribution of this thesis

The objective of this thesis is to analyse the possibilities for changing the dynamics of an MIE harvester to broaden the range of operation. Here the harvester consist of a cantilever spring with a wing attached to the the tip. Separate models of the spring and excitation are made to validate the performance of the models. As mentioned in the previous section, spring stiffeners is a method used in literature which was expected to change the range of excitation. However, this was not validated with an experimental set-up. Besides stiffness changes, changes in the mass and length will influence the eigenfrequency of the beam. Adding mass to an operational system will be hard to accomplish, but changing the length could also be considered to change the eigenfrequency of the spring. Besides changes in the dynamics of the spring, changing the excitation could also be considered as a solution.

To summarize, the contributions of this thesis are:

- separate model of the spring and aerodynamic excitation
- methods for changing the dynamics of an MIE harvester
  - changing the stiffness of the spring
  - changing the length of the spring
  - changing the excitation on the spring
- experimental validation

## 1-4 Organisation of this thesis

The remainder of this thesis has been divided into four parts:

### Chapter 2: Experimental Set-up

This chapter contains an overview of the hardware used for testing. Besides the experimental set-up, a list of parameters used for modelling the system is included as well.

### Chapter 3: System Modelling

For modelling, the system is divided into two subsystems. The first subsystem consists of a distributed beam model [15] which models a cantilevered spring. This beam model will be extended with a simple flow force estimation for aerodynamic effects [16]. The second subsystem is a free-floating flap, which is modelled by aerodynamics for airfoils with a thin variable geometry [17]. Both subsystems will be coupled with a vertical reaction force. Which means that all drag forces on the system will be neglected.

Both subsystems will be divided into three different disciplines. First mechanical, giving the relations between the deflection and forces. Where the required forces will be determined by a aerodynamic model. Finally, the electromechanical model will discuss electrical to mechanical coupling and the electrical circuit equations.

### Chapter 4: Experimental Validation

This chapter validates the obtained models. Changing the stiffness and the length of the cantilever beam will be considered for broadening the operational range. Both methods will be assessed on the feasibility for an active control application. Besides, some results of the attempts to change the excitation on the spring will be discussed.

### Chapter 5: Conclusions and Recommendations

Finally this thesis will be concluded with some conclusions and recommendations.

# Chapter 2

# Experimental Set-up

An sytem with one or more degrees of freedom is exposed to an MIE for a wide range of flow conditions. When the system has twoo degrees of freedom an instabillity is induced when the modes of the system are close to each other. This will accure for increasing flow speeds and induce negative demping to the system. The final MIE harvester design is highly inspired by the design of Brayant and Garcia [16]. This harvester consists of a flap attached to a spring with a ball bearing hinge. Energy is harvested by piezoelectric sheets on the spring. The sheets are positioned close to the support structure, where the internal momentum will be at a maximum, resulting in the design as shown in Figure 2-1. This chapter will discuss the experimental set-up used for the validation of the broad range MIE harvester. The chapter is divided in the following sections: Harvester design, Wind tunnel, Piezoelectric sheets, Sensors and Real-time environment.

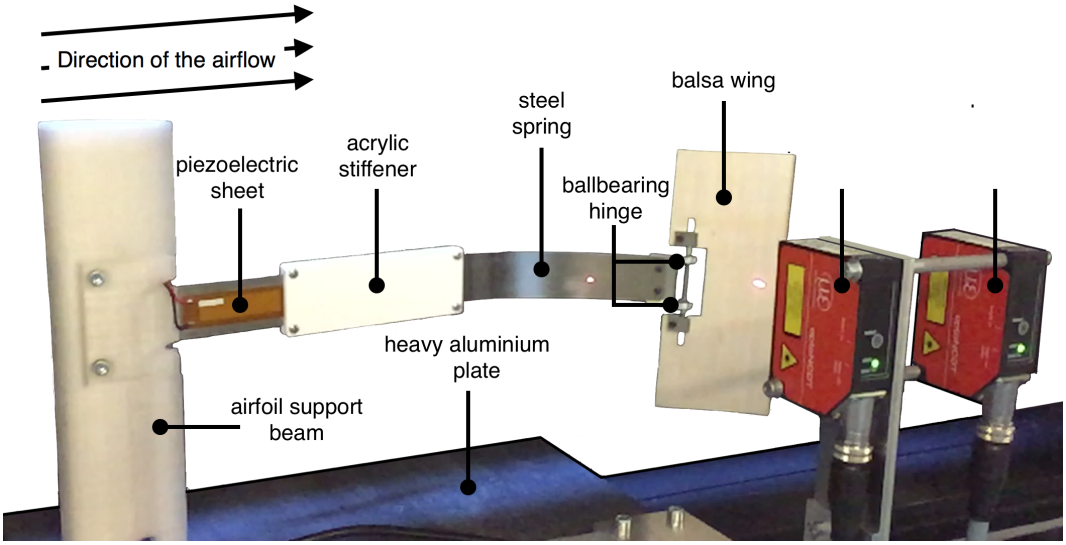


**Figure 2-1:** Photograph of the MIE harvester experimental set-up.

## 2-1 Harvester design

This section reviews the harvester design. A list of parameters used for modelling is included. Also, the differences between the original and the proposed designs will be discussed. Constants with a subscript $p$ belong to the piezoelectric sheets, subscript $a$ to the acrylic stiffener and subscript $s$ to the steel cantilever spring. When the subscript of a constant is a number, it refers to the three different cross-sections numbered from left to right. In Figure 2-2 a schematic top-view of this harvester is given. All parameters which will be needed for the harvester model are available in Table 2-1 on the next page.

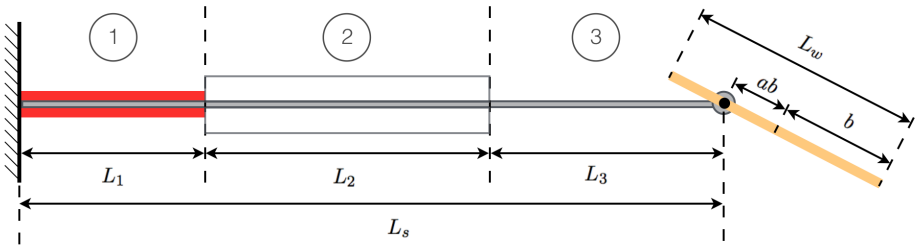


**Figure 2-2:** Schematic top-view of harvester.

The main difference of the used harvester design, with previous designs is the streamlined support structure. To reduce the impact of the support, the height of the support beam is chosen to be higher than the flap. For simplicity, the airfoil is replaced by a rigid flat plate. This might influence the performance, but will not have an influence on the proof of concept. There are also several differences in the dimensions of the harvester. The spring is slightly longer and made of a slightly thinner material. Differences in the used piezoelectric sheets will be discussed in the next section.

For both designs the wing is made of balsa wood. Balsa wood has a very high strength to weight ratio but, as with most woods, the grains have a large influence on stiffness. To create a stiff wing and prevent tearing the wing is reinforced with adhesive tape perpendicular to the grains in the wood.

## 2-2 Piezoelectric sheets

In the past piezoelectric materials have shown to be an effective way of active stiffness control [18]. Piezoelectric materials are effective because of a strong electro-mechanical coupling. Another advantage is that piezoelectric sheets can simply be glued to a surface. Coils and magnets could be used as an alternative, however piezoelectric sheets are favourable because of their low weight. Adding weight to a system will have a large influence on the eigenfrequency of the system. For the piezoelectric sheets an M4010P1 Macro Fiber Composite (MFC) sheet is used. The piezoelectric sheet is smaller than the original design.

**Table 2-1:** Parameters needed for modelling.

| Parameter | Symbol | Value | Units |
|---|---|---|---|
| Air density | $\rho_{air}$ | 1.293 | $kg/m^3$ |
| Total length | $L_s$ | 250 | $mm$ |
| Tip mass | $M_t$ | 8 | $g$ |
| Tip inertia | $J_t$ | 0 | $kgm^2$ |
| Material damping ratio | $\zeta$ | 0 | – |
| Spring width | $b_s$ | 25 | $mm$ |
| Spring thickness | $h_s$ | 0.3 | $mm$ |
| Spring density | $\rho_s$ | 7850 | $kg/m^3$ |
| Piezo length | $L_p$ | 46 | $mm$ |
| Piezo width | $b_p$ | 10 | $mm$ |
| Piezo thickness | $h_p$ | 0.3 | $mm$ |
| Piezo density | $\rho_p$ | 7700 | $kg/m^3$ |
| Stiffener length | $L_a$ | – | $mm$ |
| Stiffener width | $b_a$ | 35 | $mm$ |
| Stiffener thickness | $h_a$ | 3 | $mm$ |
| Stiffener density | $\rho_a$ | 1180 | $kg/m^3$ |
| Spring stiffness | $Y_s$ | 217 | $GPa$ |
| Piezo stiffness | $Y_p$ | 67 | $GPa$ |
| Stiffener stiffness | $Y_a$ | 3.2 | $GPa$ |
| Piezoelectric constant | $d_{31}$ | $-170$ | $pm/V$ |
| Strain permittivity | $e_{33}$ | 15.93 | $nF/m$ |
| Wing span | $s$ | 140 | $mm$ |
| Wing length | $L_w$ | 60 | $mm$ |
| Hinge position | $a$ | $-2/3$ | – |
| Semi chord | $b$ | $0.5L_w$ | $mm$ |
| Wing thickness | $h_w$ | 2 | $mm$ |
| Wing density | $\rho_w$ | 160 | $kg/m^3$ |
| Wing stiffness | $Y_w$ | 67 | $GPa$ |
| Wing mass | $M_w$ | 5.8 | $g$ |
| Wing inertia | $I_\alpha$ | 5.47 | $kgmm^2$ |
| Static unbalance | $x_\alpha$ | 0.273 | – |

## 2-3 Wind tunnel

For performance testing a closed return wind tunnel is used owned by DCSC. The maximum air speed which could be reached is 10 m/s. For calibration of the wind tunnel a Conrad Electronic Anemometer HP816A is used. After calibration an accuracy of $\pm 0.3$ m/s could be reached. To place the harvester into the wind tunnel it is fixed to a thick aluminium plate. This plate will be placed on the bottom of the wind tunnel's test section. The test section of the wind tunnel is 200 mm wide, 400 mm high and 700 mm long. In total, the circuit length of the wind tunnel is about 6 m long. Unfortunately, the wind tunnel could not be used as a closed circuit. When the wind tunnel is closed there would not be sufficient room to keep the harvester in the measurement range of the laser. Therefore one side of the wind tunnel is left open during the experiments. Figure 2-3 shows the harvester in the wind tunnel.

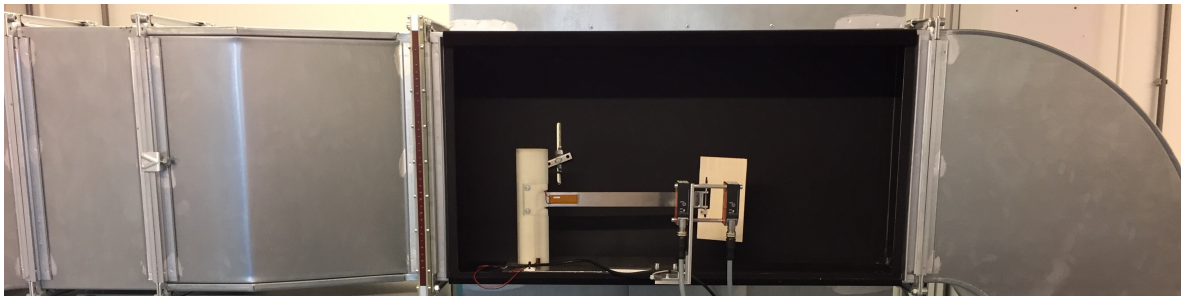

**Figure 2-3:** Photograph of the flow induced vibration energy harvester in the wind tunnel.

## 2-4 Sensors

For distance measurements on the spring and wing an optoNCDT 1302 laser is used. This sensor has a measurement rate of 750 Hz and a resolution of 30 $\mu$m. To be able to do measurements over the entire width of the wind tunnel, a measurement range of 200 mm is chosen. The purpose of the sensors is to validate the poles of the model which will be discussed in the upcoming chapters.

Besides distance measurements, a piezoelectric sheet on the outside of the wind tunnel is also used for measurements. The purpose of this sensor is to help identify modes from the wind tunnel and the harvester.

## 2-5 Real-Time environment

The data acquisition is done with a dSPACE™ system. Required data acquisition schemes are designed in Matlab™ and Simulink™. These schemes can be compiled on the dSPACE™ chip and form the real-time environment.

All inputs of the system will be connected to the Digital to Analog Conversion (DAC) ports and all outputs of the system to the Analog to Digital Converter (ADC) ports. The real-time system will run with a sampling rate of 500 Hz. A schematic representation of the system is available in Figure 2-4.

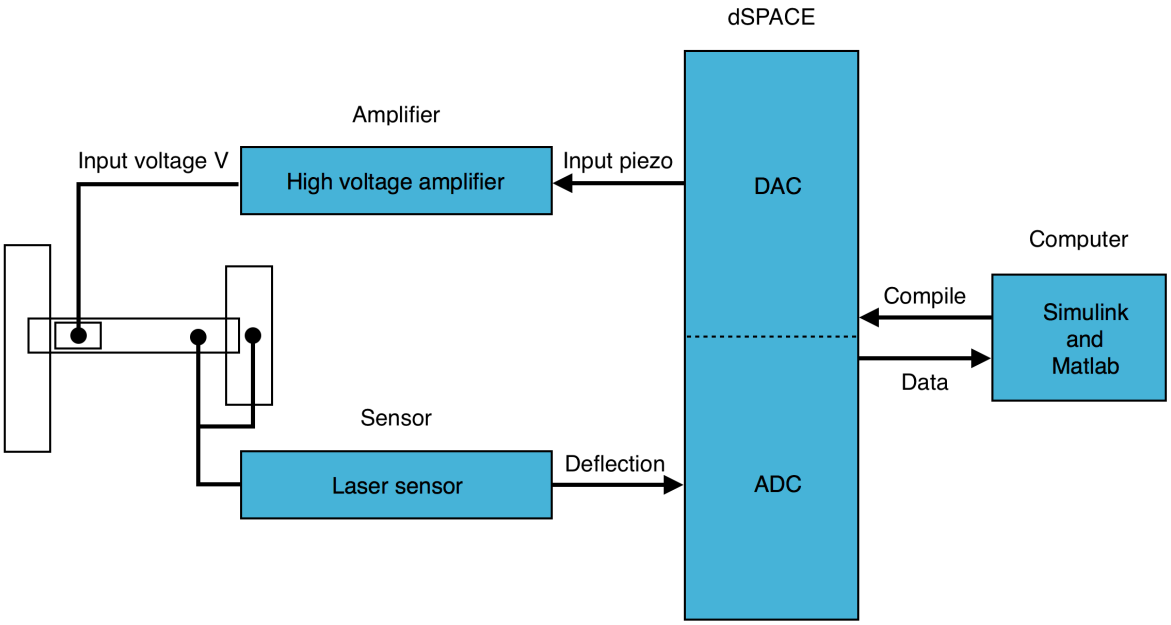


**Figure 2-4:** Schematic overview of the test set-up and real-time system.

## 2-6 Summary

This chapter introduced the MIE harvester set-up which will be used for the modelling and experimental validation. For harvesting the energy from the MIE piezoelectric sheets are used. Piezoelectric sheets are a suitable material for harvesting because of their strong electro mechanical coupling, easy attachment and low weight. During the experiments the range of wind speeds that can be used is between 1 and 10 m/s with an accuracy of $\pm 0.3$. The lasers which measure the vibration of the spring have a measurement rate of 750 Hz and a resolution of 30 $\mu$m. However, a lower sampling rate of 500 Hz will be used for the real-time system. This frequency is far above the first two eigenfrequencies of the system.

# Chapter 3

# Modelling of an MIE Harvester

For the system model a cantilevered harvester [15, 16] is combined with a flow force model [17]. To provide a good overview, the system is divided into two subsystems. These subsystems are cantilever spring and the flexible wing. Each subsystems is divided into three different disciplines. First mechanical, giving the relations between the deflection and forces, where the forces will be determined by an aerodynamic model. Finally, the electromechanical model will discuss electrical to mechanical coupling and the electrical circuit equations. In Figure 3-3 a graphical representation of the system divided into the different disciplines is given. Both models are written in a state space notation to create a set of first order differential equations.

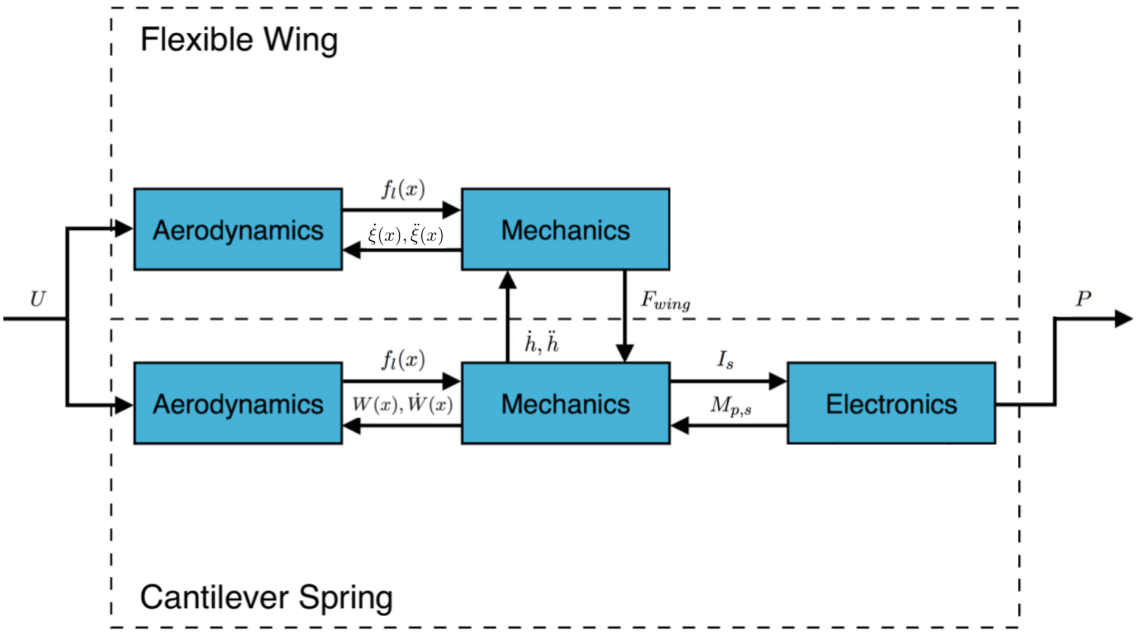


**Figure 3-1:** Block diagram of the system witch the different subsystems.

## 3-1 Modelling of the Cantilever Spring

This section will deal with the modelling of the cantilever spring. The proposed model is a distributed parameter model [15] which is based on the Euler-Bernoulli beam theory. This theory will be treated in the mechanical modelling part of this section. Followed by aerodynamic modelling where the lift force for a Bernoulli beam will be determined. The lift force is results in an aerodynamic damping and additional stiffness of the spring. In the part about electrical modelling all electrical equations of the piezoelectric material will be given. Finally, all equations will be combined into a state space model in the last part of this section.

### Mechanical modelling

In order to derive a mechanical model for the cantilever the Euler-Bernoulli beam bending theory is used [19]. Assuming the internal momentum $M(x,t)$ of the beam can be expressed with the Euler-Bernoulli equation:

$$M(x,t) = YI\frac{\partial^2 w}{\partial x^2}(x,t) \tag{3-1}$$

Where the internal momentum is a function of the transverse deflection $w(x,t)$ multiplied with the constants $Y$ and $I$, which are the Young's modulus and momentum of inertia. This results in the equation of motion for a small beam element of length $dx$:

$$\frac{\partial^2}{\partial x^2}\left[YI(x)\frac{\partial^2 w}{\partial x^2}(x,t)\right] + \rho A(x)\frac{\partial^2 w}{\partial t^2}(x,t) = f(x,t) \tag{3-2}$$

Here, $\rho(x)$ is the density, $A(x)$ is the cross-sectional area and $f(x,t)$ is an external force per unit length. However, to model a cantilever with a piezoelectric material some extensions are required. The piezoelectric material is attached on both sides of the cantilever as in Figure 2-2. Subscript $r$ is used to refer to the different cross section of the spring. Adding the piezoelectric material results in an additional internal $M_p(V,x,t)$ induced voltage $V(t)$ in the piezoelectric sheet [15].

$$M(x,t) = YI\frac{\partial^2 w}{\partial x^2}(x,t) + M_p(V,x,t) \tag{3-3}$$

$$\frac{\partial^2}{\partial x^2}\left[YI(x)\frac{\partial^2 w}{\partial x^2}(x,t)\right] + \rho A(x)\frac{\partial^2 w}{\partial t^2}(x,t) = f(x,t) - \frac{\partial^2 M_p}{\partial x^2}(x,t) \tag{3-4}$$

The fourth order differential equation is solved by using the separation principle. This comes down to define the deflection $w(x,t)$ as in equation (3-5); where $T_i(t)$ are the normal coordinates and $W_i(x)$ are the mode shapes for the $i$th mode. Note that the deflection is now expressed in two separate functions which are only dependent on time or position.

$$w(x,t) = \sum_{i=1}^{\infty} W_{ir}(x)T_i(t) \tag{3-5}$$

When (3-5) is substituted into equation (3-4) with $M_p(V,x,t)$ and $f(t)$ chosen equal to zero, the free vibration is obtained. The result of the separation principle are two separate differential equations, which are a function of position or time respectively. Note that, because of the different cross-sections the solution which is a function of position consist of separate equations. The different cross-sections are numbered from left to right by subscript $r$.

A fourth order differential equation has a solution in the form:

$$W_{ir}(x) = A_{ir}cos(\beta_{ir}x) + B_{ir}sin(\beta_{ir}x) + C_{ir}cosh(\beta_{ir}x) + D_{ir}sinh(\beta_{ir}x) \tag{3-6}$$

Where:

$$\beta_{ir}^4 = \frac{\rho_r A_r {\omega_i}^2}{Y_r I_r} \tag{3-7}$$

By enforcing the boundary and transition conditions (3-6) can be solved. First create a matrix $A_{8\times8}$ which contains all conditions when multiplied with the vector $a$ defined in (3-8). Then the eigenfrequencies $\omega_i$ can be obtained by choosing $\omega_i$ in such a way that $A$ will be singular. Finally, the values of $a$ could be obtained from the corresponding eigenvector, which spans the null space. The boundary and transmission conditions are available in the appendices (A-1)-(A-8).

$$a = \begin{bmatrix} A_{i1} & B_{i1} & C_{i1} & D_{i1} & A_{i2} & B_{i2} & C_{i2} & D_{i2} \end{bmatrix}^T \tag{3-8}$$

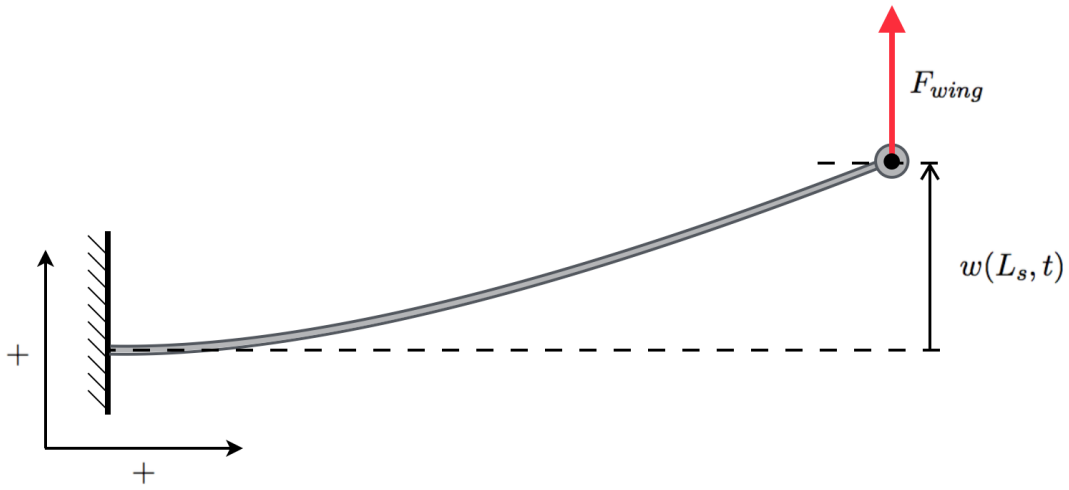


**Figure 3-2:** Free body diagram of the spring.

The equation of motion (3-9) can be obtained when (3-6) is substituted into the equation of motion, multiplied with $W_{jr}(x)$ and integrated over the entire length of the beam [19, 20]. Here the matrix $W_{jr}(x)$ should be chosen in such a way that it is orthogonal to $W_{ir}$. To model mechanical losses also an additional damping term $\zeta$ is added to the equation. Besides damping, the connection of the wing should be added to the model as well. This is done by adding the additional mass of the joint $m_{tip}$ and the lift force of the wing $F_{wing}$.

$$\sum_{i=1}^{\infty} m_i \ddot{T}_i(t) + \sum_{i=1}^{\infty} 2\zeta m_i \omega_i \dot{T}_i(t) + \sum_{i=1}^{\infty} m_i \omega_i^2 T_i(t) = \sum_{i=1}^{\infty} Q_{i,f}(x,t) - \sum_{i=1}^{\infty} Q_{i,M}(x,t) \tag{3-9}$$

Where:

$$m_i = \sum_{r=1}^{3} \rho_r A_r \int_0^{L_r} W_{ir}(x_r) W_{jr}(x_r) dx_r + m_{tip} W_{i2}(L_2) W_{j2}(L_2)$$

$$m_i \omega_i^2 = \sum_{r=1}^{3} Y_r I_r \int_0^{L_r} \frac{\partial^4 W_{ir}(x_r)}{\partial x^4} W_{jr}(x_r) dx_r$$

$$Q_{i,f}(x,t) = \sum_{r=1}^{3} \int_0^{L_r} f(x_r,t) W_{jr}(x_r) dx_i + F_{wing} W_{i2}^T(L_t)$$

$$Q_{i,M}(x,t) = \sum_{r=1}^{3} \int_0^{L_r} \frac{\partial^2 M_p}{\partial {x_r}^2}(x_i,t) W_{jr}(x_r) dx_r$$

### Aerodynamic model

A spring in an airflow will be damped by the airflow. When the angles and deflections are assumed to be linear, the aerodynamic lift force on a beam element can be estimated with the plate theory [16]. This results in an external force per unit length:

$$f(x,t) = f_{L,plate} = -0.5 \rho_{air} C_{L,plate} b_s U^2 \tag{3-10}$$

Assuming a steady flow, the lift coefficient $C_{L,plate}$ can be estimated with (3-11) [16]. Here the terms between brackets estimate the angle between the wind and spring; also known as the angle of attack. The angle of attack is estimated by the local velocity and the angle of a beam element.

$$C_{L,plate} = 2\pi \left( \left( \frac{\partial W(x)}{\partial x} T(t) \right) + \frac{W(x)\dot{T}(t)}{U} \right) \tag{3-11}$$

### Electromechanical model

The electrical-mechanical coupling results from the coupling stress $\sigma$ and voltage $V$ in a piezoelectric element. When the deformation is assumed to be in one direction, the result is the following stress strain relation [15]:

$$\sigma_1 = Y_p(\epsilon_1 - d_{31} E_3) \tag{3-12}$$

In this equation $\epsilon$ is the strain, $d_{31}$ a piezoelectric constant and $E$ the electrical field. The subscripts 1 and 3 refer to the directions. From the local stresses a local momentum can be determined. This results in a momentum which will also consist of a mechanical and electrical component. Consider only the moment as the result of the piezoelectric effect $M_p$ and write the electrical field $E_3$ in terms of a voltage $V(t)$, by the substitution of $E_3 = -V(t)/h_p$. The resulting expression is given in (3-13) where $u(x)$ is the Heaviside step function [15]. The variable $x_1$ and $x_2$ are respectively the $x$ coordinate of the begin and end of the piezoelectric sheet. Note that the distance from the centre of the piezoelectric sheet to the neutral line of the spring is $0.5(h_s + h_p)$. This can be used to determine the average strain in the piezoelectric

material. When piezoelectric sheets are placed on both sides of the spring the structure is symmetrical and for this reason the constant $\theta$ equals (3-14)[13].

$$M_p(x,t) = \theta V(t)\left(u(x-x_1) - u(x-x_2)\right) \tag{3-13}$$
$$\theta = -Y_p d_{31} b_p (h_p + h_s) \tag{3-14}$$

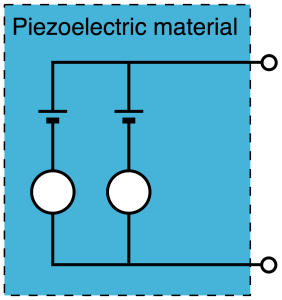


**Figure 3-3:** Schematic representation of a the two piezoelectric sheets connected in parallel.

## State space model

All equations used for modelling the cantilever motion are linear in time. When the mechanical equations of motion (3-9), the aerodynamic lift force (3-10, 3-11), and the electromechanical model (3-13) are combined the obtained relation results in (3-15).

$$\sum_{i=1}^{N_s} m_i \ddot{T}_i(t) = -\sum_{i=1}^{N_s} 2\zeta m_i \omega_i \dot{T}_i(t) - \sum_{i=1}^{N_s} m_i \omega_i^2 T_i(t) + \sum_{i=1}^{N_s} Q_{i,f}(x,t) + \sum_{i=1}^{N_s} Q_{i,M}(x,t) \tag{3-15}$$

Where:

$$Q_{i,f}(x,t) = \sum_{r=1}^{3} \int_0^{L_r} f(x_r,t) W_{ir}^T(x_r) dx_i + F_{wing}(t) W_{i3}^T(L_s$$
$$f(x,t) = -\rho_{air} \pi s_s U^2 \left( \frac{\partial W(x)}{\partial x} T(t)) + \frac{W(x)}{U} \dot{T}(t) \right)$$
$$Q_{i,M}(x,t) = \theta \frac{\partial W_{ir}^T}{\partial x}(L_p) V(t)$$
$$m_i = \sum_{r=1}^{3} \rho_r A_r \int_0^{L_r} W_{ir}(x_r) W_{ir}^T(x_r) dx_r + m_{tip} W_{i2}(L_2) W_{i2}^T(L_2)$$
$$\theta = -Y_p d_{13} b_p (h_p + h_s)$$

Note that all differential equations are linearly dependent on $g_s(t) = \begin{bmatrix} \dot{T}_i(t) & T_i(t) \end{bmatrix}^T$. This makes it possible to rewrite the equations as a set of first order equations (3-16). For coupling

the cantilever spring and the wing, the output of the system $y_s(t)$ (3-17) should be the tip displacement $h(t)$, tip velocity $\dot{h}(t)$ and tip acceleration $\ddot{h}(t)$. This can be derived by substitution of $L_s$ for $W_{ir}(x)$ in (3-5). The input of the system $u_s(t)$ consists of the resulting force of the wing $F_{wing}$ and the input voltage of the piezoelectric sheet $V(t)$. Matrices of the resulting state-space model are available in Appendices A-25 - A-33.

$$\dot{g}_s(t) = A_s g_s(t) + B_s u_s(t) \tag{3-16}$$
$$y_s(t) = C_s g_s(t) + D_s u_s(t) \tag{3-17}$$

## 3-2 Modelling of a Thin Airfoil

The aerodynamic forces of the wing are modelled with unsteady 2-D flow forces on an airfoil with a thin variable geometry [17]. This model will make it possible to analyse a rigid wing and can later be extended towards a flexible wing. This will make it possible to analyse the possibilities of controlling the poles of the system by varying the shape of the wing.

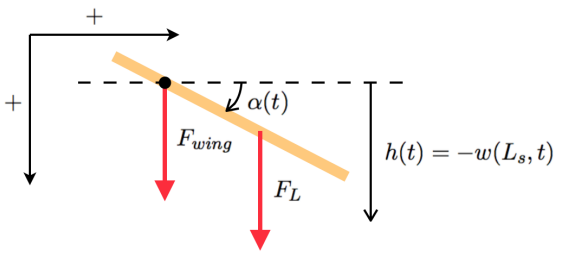


**Figure 3-4:** Free body diagram of the wing.

### Mechanical model

Given the heave $h(t)$ and pitch $\alpha(t)$, the motion of any point $\varepsilon$ on the airfoil is given by:

$$\tilde{\xi}(\varepsilon, t) = h(t) + (\varepsilon - ab)\alpha(t) \tag{3-18}$$
$$\tilde{\xi}(x, t) = h(t) + b(x - a)\alpha(t) \tag{3-19}$$

Two vertical forces will act on the wing. A lift force $F_L(t)$ as a result of the airflow and a force $F_{wing}(t)$ as a result of the deflection. The acceleration is derived by taking the second derivative of the displacement (3-19). Implementation in the Newton equation will result in (3-20).

$$\int_{-b}^{b} m(\varepsilon)\ddot{\tilde{\xi}}(\varepsilon, t)d\varepsilon = F_L(t) + F_{wing}(t) \tag{3-20}$$

For the Euler equation around the hinge is determined in a similar fashion. Now, the moment $M_L(t)$ is the moment resulting from the air flow. Only now the inertial term is with respect to the point of rotation. The spring connection will have a negligible influence, because of negligible friction in the bearings.

$$\int_{-b}^{b}(\varepsilon - ab)m(\varepsilon)\ddot{\xi}(\varepsilon/b,t)d\varepsilon = M_L(t) \tag{3-21}$$

### Aerodynamic model

In the work of Theodorsen [21] the airfoil is modelled by the thin airfoil theory. This means that the deformation of the airfoil equals the deformation of the camber line. Other assumptions are incompressible, irrotational, inviscid fluid and 2D flow [17]. Furthermore, a vortex is assumed to move with free stream velocity. The local flow force is determined by the local pressure. These pressures can be derived by the unsteady Bernoulli equation, which couples pressure to the local velocity. Local surface velocities can be described by the potential flow theory.

In the case of a rigid wing the lift force $F_L(t)$ and lift momentum $M_L(t)$ can be derived with the unsteady aerodynamics of Theodorsen. For the interested reader an extensive derivation of Theodorsen's method is available in Appendix B. The results of the method are:

$$\begin{aligned} F_L(t) &= -\pi\rho_{air}sb^2\left(U\dot{\alpha}(t) - ab\ddot{\alpha} + \ddot{h}(t)\right) - 2\pi\rho_{air}sbUCQ(t) \\ M_L(t) &= -\pi\rho_{air}sb^2\left(bU\left(0.5-a\right)\dot{\alpha}(t) + b^2\left(0.125+a^2\right)\ddot{\alpha}(t) - ab\ddot{h}(t)\right) \\ &\quad + 2\pi\rho_{air}sb^2U(0.5+a)CQ(t) \end{aligned}$$

Where the constant $\rho_{air}$ is the air density, $U$ the free streem velocity and $h(t)$ the displacement of the wing. The variable $CQ(t)$ models the wake effect and depends on the constants $A_i$, $b_i$ and variable $z_i(t)$ (3-22)[17]. Subscript $i$ represents the mode of the wake model. In order to get a first order equation $z_i$ is written as in (3-24). For a second order flat plate model the constants should be chosen equal to $A_1 = 0.165$, $A_2 = 0.335$, $b_1 = 0.0455$ and $b_2 = 0.3000$ [22].

$$CQ(t) = Q(t)(1 - \sum_i A_i) + \sum_i z_i \tag{3-22}$$

$$Q(t) = U\alpha(t) + \dot{h}(t) + (0.5-a)b\dot{\alpha}(t) \tag{3-23}$$

$$\dot{z}_i = \frac{1}{b}b_iA_iUQ(t) - \frac{1}{b}b_iUz_i \tag{3-24}$$

Changing the excitation on the spring can be done by a change in stiffness of the wing. When the stiffness of an airfoil is decreased the flutter velocity also decreases [17]. To analyse this phenomenon the orthogonal vibration modes of the wing will be added to the motion of the wing. Where the wing is modelled by two beams clamped at the position of the hinge. For a uniform clamped-free beam the first eigenfrequency can be estimated by (3-25) [19].

$$\omega = 1.875^2\sqrt{\frac{EI}{\rho Al^4}} \tag{3-25}$$

Because of the large difference in length between the spring and wing both first eigenfrequencies will be far apart. This will result in high damping values for the combined system and for this reason no limit-cycle vibration of the piezoelectric sheets on the spring. Furthermore, changing the stiffness of the wing, with for example, piezoelectric sheets require power. Passive electric circuits, also known as shunts, will only add additional damping [18]. Both methods require electric power transfer across the hinge, which is not considered as a feasible solution. Other methods for changing the dynamics of the wing might be available. However, these methods will also require power which will be hard to transfer across the hinge.

### State space model

In this subsection a first order state space model for the flow forces on a rigid thin airfoil will be obtained. Here the input of the system is the tip displacement of the cantilever spring. The desired output of the system will be the force $F_{wing}$ on the spring. This is achieved by combining (3-20), (3-21), (3-22) and (3-24). All equations dependent linearly in time on the system states $g_w(t) = [\dot{\alpha}(t) \quad \alpha(t) \quad z(t)]^T$ and the input $H(t) = [\ddot{h}(t) \quad \dot{h}(t) \quad w_{laser}]^T$. The equations can be written in the form (3-26,3-27). The matrices are available in appendices A-34-A-42.

$$\dot{g}_w(t) = A_w g_w(t) + B_w H(t) \tag{3-26}$$

$$F_{wing}(t) = C_w g_w(t) + D_w H(t) \tag{3-27}$$

## 3-3 Conclusion

Obtained equations seem to correspond with the work of Bryant and Garcia [12]. However, both methods use a different method for modelling the wake effect. Where the model used by Bryant and Garcia is based on an infinite series, Gaunaa used a model which is determined by an experimental fit. This results in different expressions for the lag states $z_i$ and $\lambda$. The lag states $z_i$ are dependent on $Q$ where the states $\lambda$ depend on $\dot{Q}$ instead. When both methods are simulated for an arbitrarily chosen $\alpha(t)$ and $h(t)$ signal, the resulting wake effects $CQ(t)$ will be similar for both models.

Experimental fit model used by Gaunaa [17]:

$$CQ(t) = Q(t)(1 - \sum_i A_i) + \sum_i z_i \tag{3-28}$$

$$\dot{z}_i = \frac{1}{b} b_i A_i U Q(t) - \frac{1}{b} b_i U z_i \tag{3-29}$$

Infinite series model used by Bryant and Garcia [16]:

$$CQ(t) = Q(t) - \frac{1}{2} \sum_{n=1}^{N_w} b_n \lambda_n(t) \tag{3-30}$$

$$A\dot{\lambda}(t) = c\dot{Q}(t) - \frac{U}{b}\lambda(t) \tag{3-31}$$

Changing the excitation on the spring is no longer seen as a feasible solution for increasing the range of harvesting. The required power for changing the dynamics of the wing could not be transferred across the hinge of the harvester. For this reason, only changing the stiffness and length of the spring will be considered for changing the range of harvesting.

# Chapter 4

# Experimental Verification

The linear state space models determined in the previous chapter will be verified in this chapter. This will be done for the spring subsystem and the combined model. In order to compare the eigenfrequencies of the model with the experimental values, spectral analysis is used (see Appendix C-1). Subsequently, the eigenfrequencies of the system are found for the peak values in the power spectrum. For the connection of both previously derived subsystems a name based connect function is used. Finally, the results will be used to determine feasibility of an effective flow induced energy harvester for a broad range of flow speeds.

## 4-1 Validation of the spring model

For experimental validation the spring is placed in the wind tunnel and the piezoelectric sheets are excited with a pseudorandom binary signal (see Figure 4-1). The signal has an amplitude of 200 V and a maximum switching rate of 20 Hz. A white noise signal will be preferred above a pseudorandom binary signal, however inapplicable through physical constraints. The spring will be excited for a duration of 120 s for a range of wind speeds between 1 and 10 m/s.

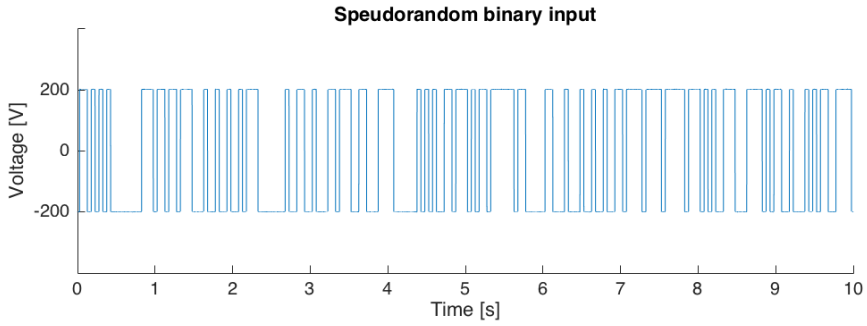


**Figure 4-1:** Pseudorandom binary input voltage on the piezoelectric sheet.

From the experimental data power spectra are created. These power spectral densities for the different wind speeds are combined in a rainflow diagram as shown in Figure 4-2. A rainflow diagram is a 3D figure with the variables frequency, spectral density and in this case wind speed on the axis. Figure 4-2 shows a top view, with the wind speed and frequency on the x- and y-axis.

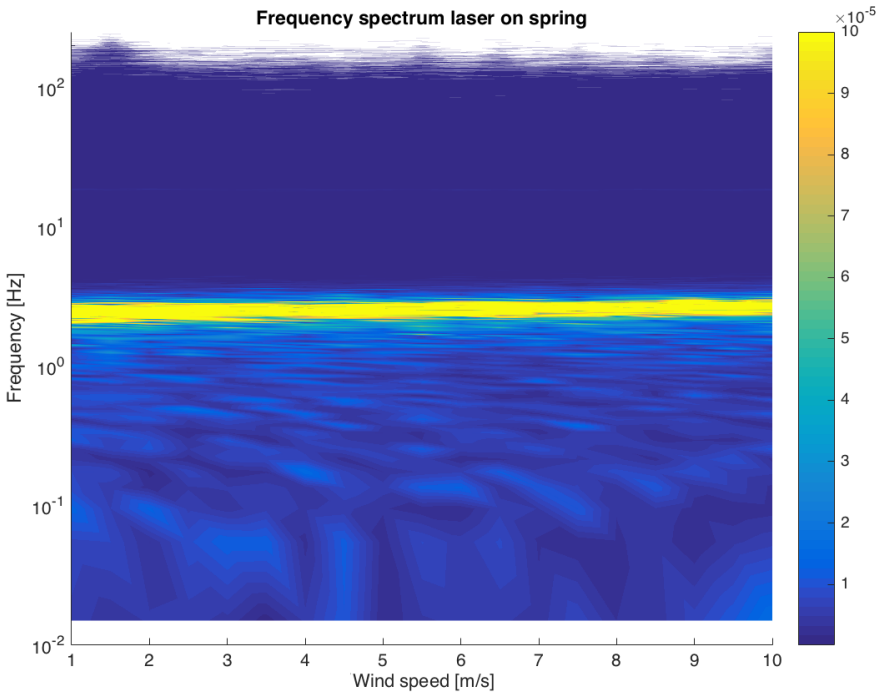


**Figure 4-2:** Rainflow diagram with a averaging factor 4 for U=1 to U=10 m/s.

When the experimental eigenfrequencies are compared with the estimated eigenfrequencies, both show a minor increase in eigenfrequency, see Figure 4-3. The error between the experimental and estimated eigenfrequency of the spring stays below 2% of the estimated value for the entire range of flow speeds.

The obtained values of the eigenfrequencies are used to fit a second order transfer function (4-1) on the experimental data. Here $\omega$ is the first eigenfrequency, $\zeta$ the damping ratio of the system and $\gamma$ the gain. For validation of the second order fit the variance accounted for (4-2) is used. The VAF compares the variance in the estimated data $y_e$ with the experimental data $y$. Often, a margin of 80% is taken for a proper fit. Figure 4-4 shows that the majority of the second order transfer functions have a VAF value above 80%.

$$G_s(s) = \frac{\gamma}{s^2 + 2\zeta\omega s + \omega^2} \tag{4-1}$$

$$VAF = \left(1 - \frac{var(y - y_e)}{var(y)}\right) 100\% \tag{4-2}$$

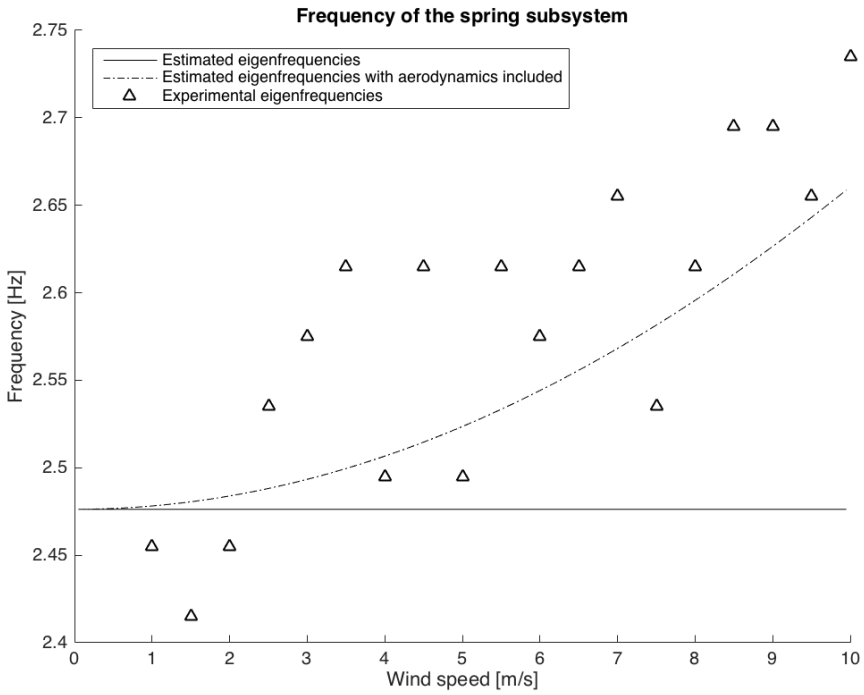


**Figure 4-3:** Eigenfrequencies of the cantilever spring for wind speeds from U=0 to U=10 m/s.

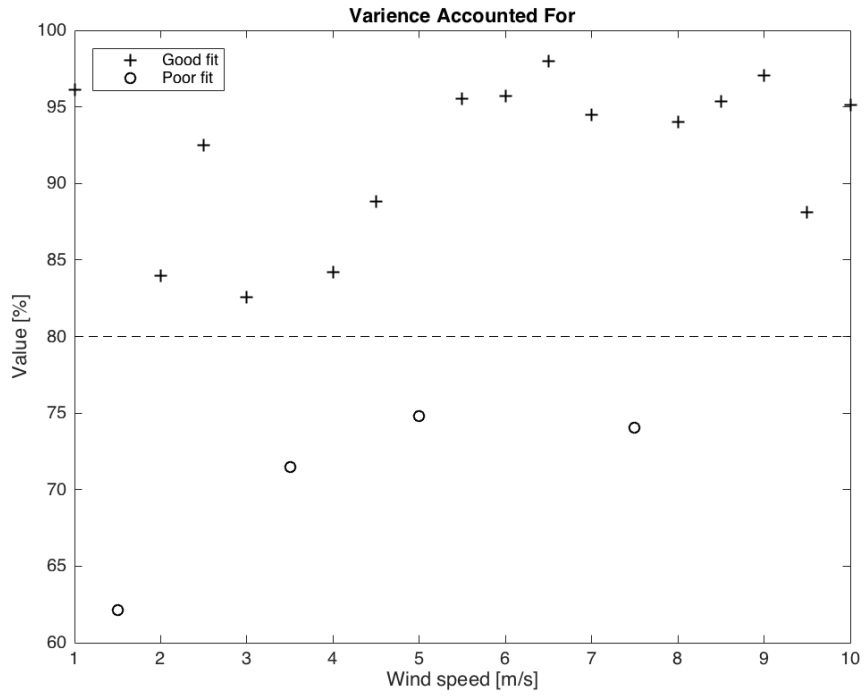


**Figure 4-4:** VAF of the of the second order transfer function fit, for wind speeds from U=0 to U=10 m/s.

When the damping and gain of the second order transfer function is compared to the spring model. Both seem to correspond in magnitude (see Figure 4-5 and Figure 4-6). However, when the wind speed increases the damping of the model is overestimated. This might be an effect of the opening in the wind tunnel, but is more likely a result of the wake effects which will reduce the aerodynamic forces on the spring [23]. For an improvement, the damping could be estimated dependent on the wind speed with a second order function. This function could be fit to the experimental data to give an improved fit for the entire range of flow speeds. Alternatively, the wake affects can also be modelled with the theory of Gaunaa [17]. Besides the error in the estimated damping, the error in the estimated gain is significant as well. This is probably the result of poor specification on the used materials or degradation during operation. When required this could be resolved by including a parameter estimation.

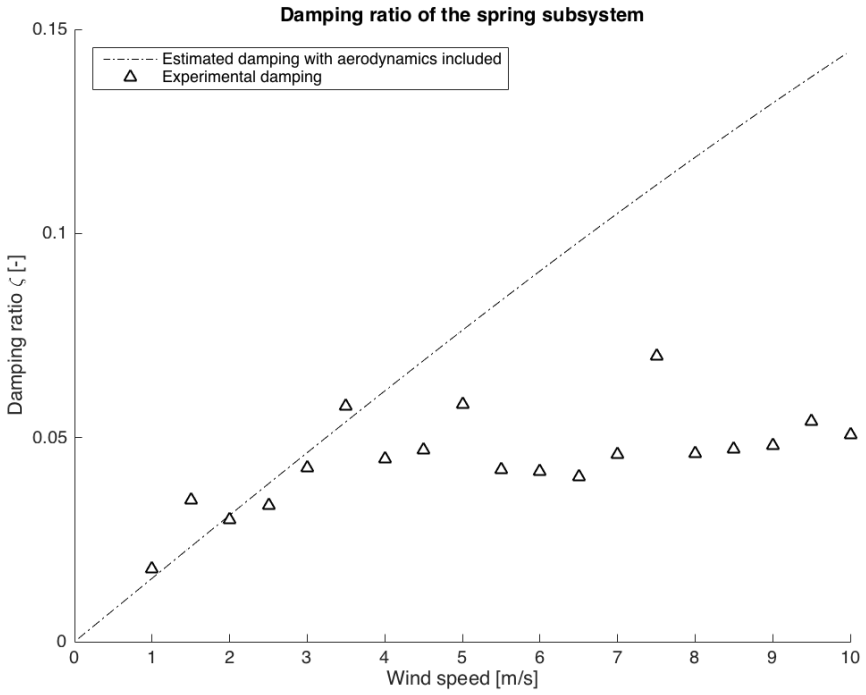


**Figure 4-5:** Damping of the spring model compared to a second order transfer function fit, for wind speeds from U=0 to U=10 m/s.

Summarizing the obtained results of the spring model validation the estimated eigenfrequency seems to estimate the trend and value of the experimental data. However, the trend in the estimated damping does not correspond to the experimental values. The overestimation of the damping might result in the underestimation of the amount of damping which could be added to the system for energy harvesting. Besides, a parameter estimation also will be required to get a more accurate model of the spring subsystem.

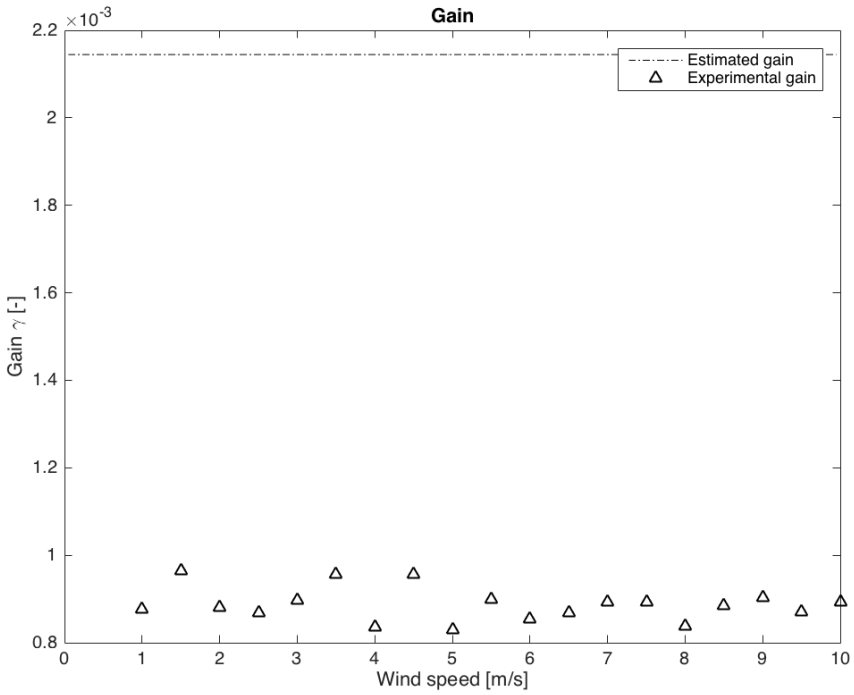


**Figure 4-6:** Gains of the spring model compared to a second order transfer function fit, for wind speeds from U=0 to U=10 m/s.

## 4-2 Validation of the connected model

The harvester is placed in the wind tunnel, with wind speeds between 1 and 10 m/s, while the piezoelectric sheets are excited by a pseudorandom binary signal with an amplitude of 100 V and a maximum frequency of 50 Hz. The resulting power spectral density of the movement of the spring is available in Figure 4-7. Here the first and second mode are clearly visible as two almost horizontal lines. Besides the modes of the spring, two modes can be observed who depend linearly on the flow velocity. This could be explained by vortex shedding at the tip of the support beam. The vortex shed frequency is linearly dependant on the flow velocity. Slow motion videos of the wing show larger deflections at the top than at lower parts of the wing. Finally, these vortices could only excite the wing and will, for this reason, not be observed in the power spectrum of the spring.

Unfortunately, the estimations for the connected system do not correspond to the experimental observations. For example, when the estimated first eigenfrequency of the spring is compared with the experimental, see Figure 4-8. For low wind speeds the estimated eigenfrequency is only a few percentages off. However, when the flow speed increases the estimated eigenfrequency increases much faster than observed in experiments. This probably also can be improved by performing an parameter estimation. Some parameters have a large influence on the dynamic behaviour of the system. Even small changes will have significant influence on the dynamics.

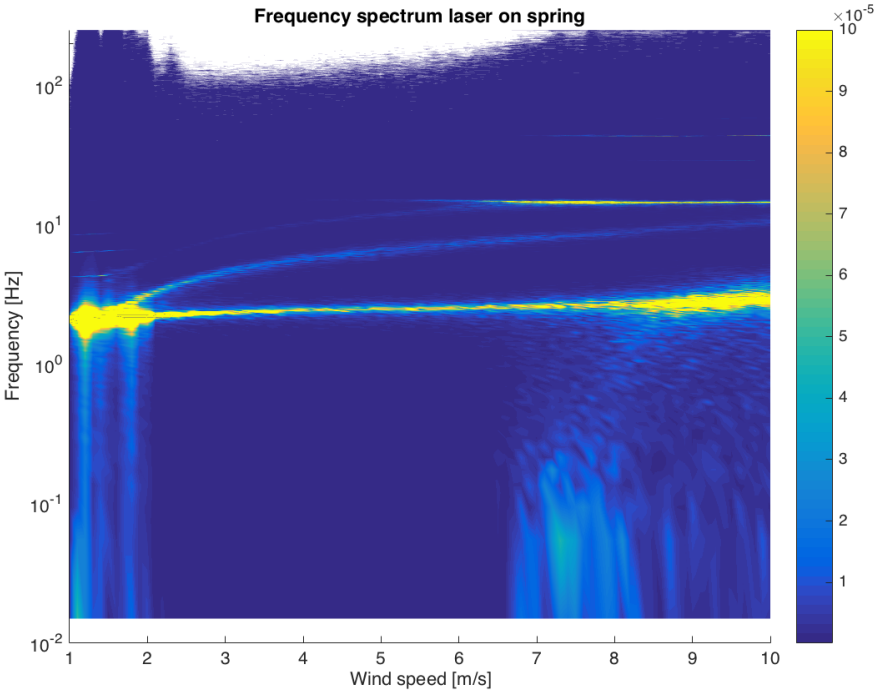


**Figure 4-7:** Rainflow of the laser on the spring, for harvester with wing.

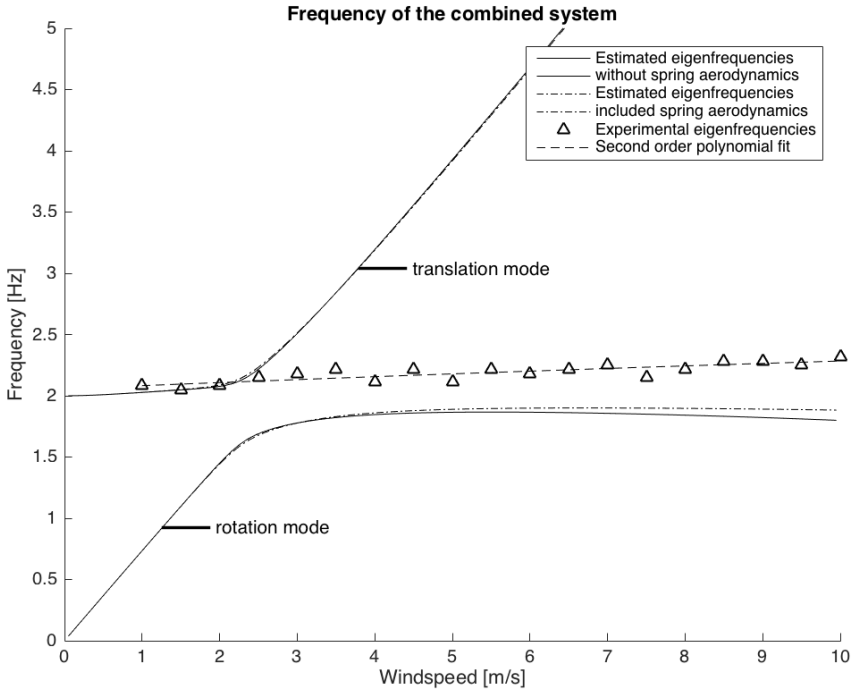


**Figure 4-8:** Frequency of first eigenmode of the spring and aerodynamic mode.

Limit cycle vibrations in the system can be observed in Figure 4-7 by higher spectral densities around the eigenfrequencies of the beam, which is the case for wind speeds from 1 up to 2 m/s. For this wind speeds the first mode of the spring can be observed. For higher wind speeds the aerodynamic modes will excite the second mode of the spring. This results in an increase in the power spectrum of both eigenfrequencies of the spring.

The connected system estimates a stable system as showed in Figure 4-9. Despite this, the model estimates a small decrease in damping for flow speeds around 3 m/s. The system stays clear from the zero-damping line and was estimated as a stable system for the entire range of flow speeds. However, in practice the system shows limit cycle behaviour for wind speeds up to 2 m/s. Even at very low wind speeds (0.2 m/s measured with the Conrad Electronic Anemometer HP816A) the system stays in a constant vibration. Of course, this could be explained by the additional modes observed in the rainflow. If these modes indeed are the result of vortex shedding, this could be a source of excitation, which potentially keeps the system in limit cycle vibrations.

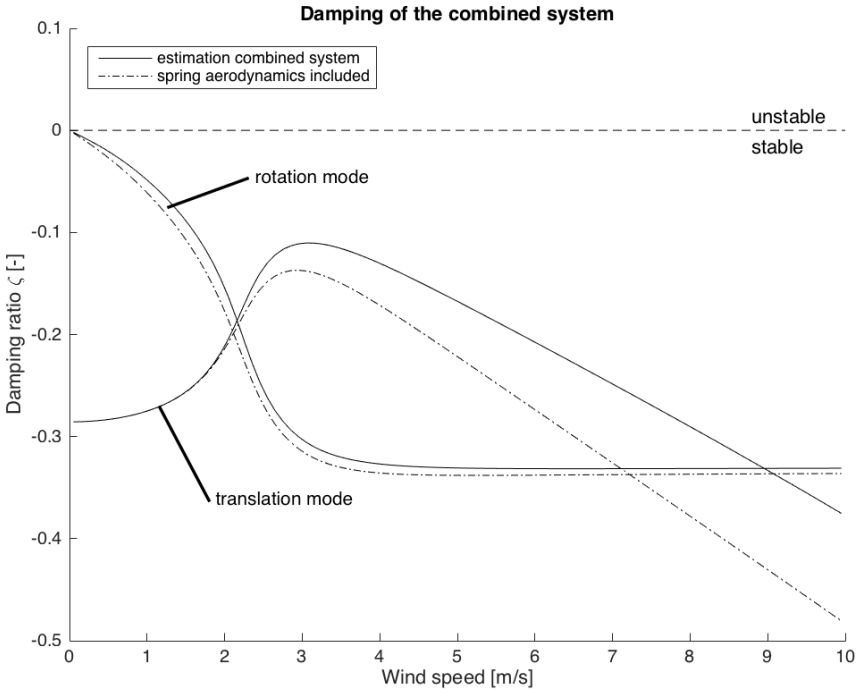


**Figure 4-9:** Damping of first mode of the spring the and aerodynamic mode for a wind speed of U=0 to U=10 m/s.

## 4-3 Changing the eigenfrequency of the cantilever spring

In the introduction, three methods for increasing the operational range of harvesting were considered. After excluding changing the excitation in the previous chapter, the remaining options are:

- changing the stiffness of the cantilever spring
- changing dimensions of the cantilever spring

## Stiffness change

Changing the stiffness with beam stiffeners was expected to have a large influence on harvesting dynamics for MIE and IIE harvesters [13]. Although stiffeners revealed useful in an experimental validation for an IIE harvester, the effect on an MIE harvester is disappointing. Figure 4-10 shows the estimated and experimentally determined eigenfrequencies of a spring with different stiffener lengths of acrylic glass. The experimental values of the eigenfrequencies show the same behaviour as the estimated frequencies. However, the change in eigenfrequeuncy is lower than expected.

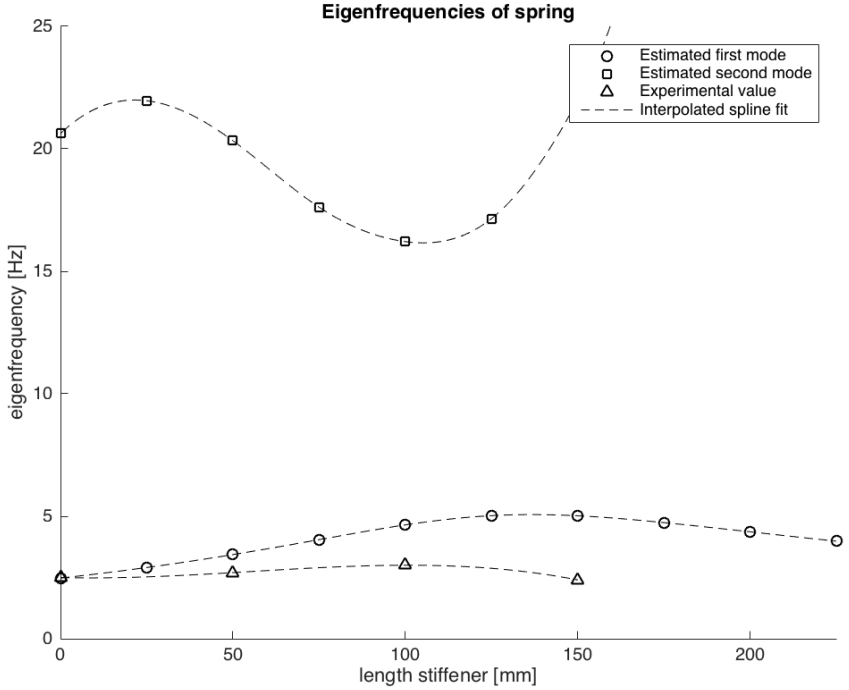


**Figure 4-10:** Eigenfrequencies of the spring for different length of the beam stiffener.

For the harvester with the beam stiffener an increase in the first eigenfrequency of the spring can be observed. Besides the increase in eigenfrequency, an increase in the range of flow speeds which leads to oscillations can be observed. However, with an inaccuracy of 0.6 m/s this increase is not significant. The second eigenfrequency of the spring was decreased by the beam stiffener. This decrease in frequency results in an excitation for lower flow speeds. When the harvester vibrates in the second eigenfrequency of the spring, unfortunately a movement of the entire harvester set-up is induced as well. This results in noise on the lasers, which are attached on the plate of the harvester set-up. The noise also could be observed in the rainflow available in Figure 4-11

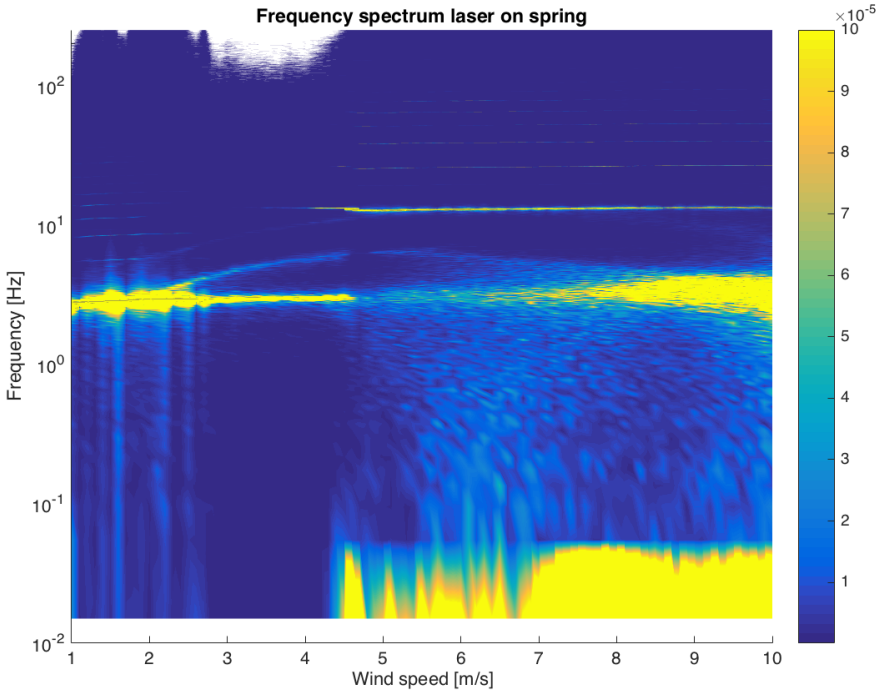


**Figure 4-11:** Power spectral density of the laser on the spring. The stiffness of the beam is increased with a acrylic glass stiffener of 100 mm.

## Length change

The MIE harvesters designed by Bryant and Garcia had an eigenfrequency around 4 Hz [16]. This is almost twice the eigenfrequency of the harvester designed for this investigation, which is a result of the choice for a slightly longer and thinner material for the spring. Comparing both designs a large difference in the operational range can be observed. Where the original harvester design was capable of harvesting energy for wind speeds between 2 and 9 m/s. The new design, with the lower eigenfrequency, was only capable of harvesting between wind speeds of 1 and 2 m/s. When the spring was replaced by a spring comparable in thickness and length the range of limit cycle oscillations increased. However, there have been no extensive experiments with different lengths of springs. This method seems more effective in changing the eigenfrequency of the spring. For a harvester capable of changing length a modification in the design will be required as the piezoelectric sheets should be at the root of the spring for optimal performance.

# Chapter 5

# Conclusion and Recommendations

The objective of this thesis was to analyse the possibilities for changing the feasibility of a broad range flow induced vibration harvesting device. Beam stiffeners have been proposed in recent literature. However, changing the length and aerodynamics of the excitation were considered to be a solution as well. Linear state space models have been created and experimental verifications have been performed. Leading to the following conclusion and recommendations.

## 5-1 Conclusion

### Changing the operational range with stiffeners

Although simulations with stiffeners resulted in differences in the operational range of an MIE harvester [13], experimental results contradict this estimation. Besides, the expected change in eigenfrequency was not supported by the experiments. However, beam stiffeners might have some positive effects on the efficiency because of changes in the mode shapes. Stiffeners do not seem a usable method for actively changing the operational field of an MIE energy harvester.

### Changing the operational range by length changes

Changes in the length and thickness of the cantilever spring have an influence on the eigenfrequency of the harvester. Besides, a shift in the operational field was observed as well. However, if the change in operational field also has a positive influence on the energy which can be extracted from the harvester remains to be investigated. Despite that a change in size might be difficult to implement, because of the piezoelectric sheets, the method seems the most effective in changing the operational range of an MIE harvester.

### Changing the operational range by changing the excitation

When the stiffness of an airfoil is reduced the critical flow speed loading to limit cycle oscillations will reduce [17]. However, changing the stiffness or shape of a wing does not seem to be a feasible solution. Besides, the length of the wing is short compared to the length of the spring. This means a large difference in eigenfrequencies resulting in high damping values.

## 5-2 Recommendations

### Design improvements

Despite an uniform airfoil as a support beam the harvester still seems to be excited by a vortex from the top of the support beam. When the vortex shedding of the top of the support beam is indeed the cause of the excitation the solution is very simple: only the length of the support beam should be increased and the problem would be solved. There are several observations which support the vortex shedding theory:

- linearly on the flow velocity
- slow motion videos show larger deflections at the top than at lower parts of the wing
- only excite the wing that reaches a comparable height

Besides the improvement on the support beam also an alternative way of fixing the harvester should be considered. When the harvester was in a limit-cycle oscillation the heavy plate on the bottom of the wind tunnel started vibrating as well. These undesired vibrations also disturbed the measurements, due to vibrations in the support structure of the lasers.

### Model improvements

The obtained model for the spring seems to be effective in estimating the trends in the dynamics of the system. However, the damping of the system is over estimated, which might result in the underestimation of the amount of energy available for harvesting. Parameter estimation could be a solution to improve the model. Even a simple first order transfer function was capable of modelling the dynamics of the system.

For the combined model also an parameter estimation could be performed for improving the model. However when the excitation of the system is indeed a result of vortex shedding, this will be included in the parameters of the estimation. To prevent this from happening, first the design should be improved.

### Implementation of additional damping

Piezoelectric materials have been applied as sensors and actuators for vibration control [18]. Besides active feedback control, passive electrical circuits called shunts can also be designed

to damp vibrations. These shunts are particularly attractive for energy harvesters because these systems will not require energy that has to be put into the system.

When only a resistor is connected to the piezoelectric sheets to extract energy from the system this will only add minor damping to the system. The damping on the system is equivalent to that of a light visco-elastic material [18]. Pure resistor shunts will not add significant amounts of damping, because of the fixed gain. However, it is claimed that adding an inductor is claimed might improve the damping.

# Appendix A

# Full Mechanical Expressions

## Mechanical model of the cantilever spring

### Boundary and transmission conditions for two different cross-sections

Boundary conditions for a beam clamped at $x_1 = 0$ and free at $x_2 = L_s - L_p$. Completed with the transmission conditions for $x_1 = L_p$ and $x_2 = 0$.

$$w_1(0,t) = 0 \tag{A-1}$$

$$\frac{\partial w_1(x_1,t)}{\partial x_1}|_{x_1=0} = 0 \tag{A-2}$$

$$Y_2 I_2 \frac{\partial^2 w_2(x_2,t)}{\partial x_2^2}|_{x_2=L_2} = -J_t \frac{\partial^3 w_2(x_2,t)}{\partial x_2 \partial t^2}|_{x_2=L_2} \tag{A-3}$$

$$Y_2 I_2 \frac{\partial^3 w_2(x_2,t)}{\partial x_2^3}|_{x_2=L_2} = M_t \frac{\partial^2 w_2(x_2,t)}{\partial t^2}|_{x_2=L_2} \tag{A-4}$$

$$w_1(L_1,t) = w_2(0,t) \tag{A-5}$$

$$\frac{\partial w_1(x_1,t)}{\partial x_1}|_{x_1=L_1} = \frac{\partial w_2(x_2,t)}{\partial x_2}|_{x_2=0} \tag{A-6}$$

$$Y_1 I_1 \frac{\partial^2 w_1(x_1,t)}{\partial x_1^2}|_{x_1=L_1} = Y_2 I_2 \frac{\partial^2 w_2(x_2,t)}{\partial x_2^2}|_{x_2=0} \tag{A-7}$$

$$Y_1 I_1 \frac{\partial^3 w_1(x_1,t)}{\partial x_1^3}|_{x_1=L_1} = Y_2 I_2 \frac{\partial^3 w_2(x_2,t)}{\partial x_2^3}|_{x_2=0} \tag{A-8}$$

### Boundary and transmission conditions for two different cross-sections

Boundary conditions for a beam clamped at $x_1 = 0$ and free at $x_3 = L_3 = L_s - L_p - L_c$. Completed with the transmission conditions for $x_1 = L_1 = L_p$ $x_2 = 0$ and $x_2 = L_2 = L_c$

$x_3 = 0$.

$$w_1(0,t) = 0 \tag{A-9}$$

$$\frac{\partial w_1(x_1,t)}{\partial x_1}|_{x_1=0} = 0 \tag{A-10}$$

$$Y_3 I_3 \frac{\partial^2 w_3(x_3,t)}{\partial x_3^2}|_{x_3=L_3} = -J_t \frac{\partial^3 w_3(x_3,t)}{\partial x_3 \partial t^2}|_{x_3=L_3} \tag{A-11}$$

$$Y_3 I_3 \frac{\partial^3 w_3(x_3,t)}{\partial x_3^3}|_{x_3=L_3} = M_t \frac{\partial^2 w_3(x_3,t)}{\partial t^2}|_{x_3=L_3} \tag{A-12}$$

$$w_1(L_1,t) = w_2(0,t) \tag{A-13}$$

$$\frac{\partial w_1(x_1,t)}{\partial x_1}|_{x_1=L_1} = \frac{\partial w_2(x_2,t)}{\partial x_2}|_{x_2=0} \tag{A-14}$$

$$Y_1 I_1 \frac{\partial^2 w_1(x_1,t)}{\partial x_1^2}|_{x_1=L_1} = Y_2 I_2 \frac{\partial^2 w_2(x_2,t)}{\partial x_2^2}|_{x_2=0} \tag{A-15}$$

$$Y_1 I_1 \frac{\partial^3 w_1(x_1,t)}{\partial x_1^3}|_{x_1=L_1} = Y_2 I_2 \frac{\partial^3 w_2(x_2,t)}{\partial x_2^3}|_{x_2=0} \tag{A-16}$$

$$w_2(L_1,t) = w_3(0,t) \tag{A-17}$$

$$\frac{\partial w_2(x_2,t)}{\partial x_2}|_{x_2=L_2} = \frac{\partial w_3(x_3,t)}{\partial x_3}|_{x_3=0} \tag{A-18}$$

$$Y_2 I_2 \frac{\partial^2 w_2(x_2,t)}{\partial x_2^2}|_{x_2=L_2} = Y_3 I_3 \frac{\partial^2 w_3(x_3,t)}{\partial x_3^2}|_{x_3=0} \tag{A-19}$$

$$Y_2 I_2 \frac{\partial^3 w_2(x_2,t)}{\partial x_2^3}|_{x_2=L_2} = Y_3 I_3 \frac{\partial^3 w_3(x_3,t)}{\partial x_3^3}|_{x_3=0} \tag{A-20}$$

## Local stiffness and mass

Local stiffness and mass for different cross-sections (A-1)-(A-8) are:

$$\begin{aligned}
Y_1 I_1 &= Y_s b_s \frac{{h_s}^3}{12} + 2 Y_p b_p \frac{(h_p + 0.5 h_s)^3 - 0.125 {h_s}^3}{3} \\
\rho_1 A_1 &= \rho_s h_s b_s + 2 \rho_p h_p b_p \\
Y_2 I_2 &= Y_s b_s \frac{{h_s}^3}{12} \\
\rho_2 A_2 &= \rho_s h_s b_s
\end{aligned}$$

Local stiffness and mass for different cross-sections (A-9)-(A-20) are:

$$
\begin{aligned}
Y_1 I_1 &= Y_s b_s \frac{{h_s}^3}{12} + 2 Y_p b_p \frac{(h_p + 0.5 h_s)^3 - 0.125 {h_s}^3}{3} \\
\rho_1 A_1 &= \rho_s h_s b_s + 2 \rho_p h_p b_p \\
Y_2 I_2 &= Y_s b_s \frac{{h_s}^3}{12} + 2 Y_c b_c \frac{(h_c + 0.5 h_s)^3 - 0.125 {h_s}^3}{3} \\
\rho_2 A_2 &= \rho_s h_s b_s + 2 \rho_c h_c b_c \\
Y_3 I_3 &= Y_s b_s \frac{{h_s}^3}{12} \\
\rho_3 A_3 &= \rho_s h_s b_s
\end{aligned}
$$

# Mechanical model of the wing

## Masses and inertias

$$\int_{-b}^{b} m(\varepsilon) \ddot{\xi}(\varepsilon, t) d\varepsilon = M_{wing} \ddot{h}(t) + M_{wing} (\varepsilon_{cg} - ab) \ddot{\alpha}(t) \tag{A-21}$$

$$\varepsilon_{cg} = \frac{1}{M_{wing}} \int_{-b}^{b} \varepsilon m(\varepsilon) d\varepsilon \tag{A-22}$$

$$\int_{-b}^{b} (\varepsilon - ab) m(\varepsilon) \ddot{\xi}(\varepsilon/b, t) d\varepsilon = (\varepsilon_{cg} - ab) M_{wing} \ddot{h}(t) + I_\alpha \ddot{\alpha}(t) \tag{A-23}$$

$$I_\alpha = I_{cm} + (\varepsilon_{cm} - ab)^2 M_{wing} \tag{A-24}$$

## State-space of the spring

Rewrite (3-10) in the notation:

$$f_l = f_{l\zeta 1}\dot{T}_1(t) + f_{l\omega 1}T_1(t) + \cdots + f_{l\zeta Ns}\dot{T}_{Ns}(t) + f_{l\omega Ns}T_{Ns}(t) \tag{A-25}$$

$$f_{l\zeta 1} = -\frac{\rho_{air}s_s U^2\pi}{m_1}\sum_{r=1}^{3}\int_0^{L_r} W_{1r}(x)W_{1r}(x)dx \tag{A-26}$$

$$f_{l\omega 1} = -\frac{\rho_{air}s_s U\pi}{m_1}\sum_{r=1}^{3}\int_0^{L_r} \partial W_{1r}(x)W_{1r}(x)dx \tag{A-27}$$

$$f_{l\zeta Ns} = -\frac{\rho_{air}s_s U^2\pi}{m_{Ns}}\sum_{r=1}^{3}\int_0^{L_r} W_{Nsr}(x)W_{1r}(x)dx \tag{A-28}$$

$$f_{l\omega Ns} = -\frac{\rho_{air}s_s U\pi}{m_{Ns}}\sum_{r=1}^{3}\int_0^{L_r} \partial W_{Nsr}(x)W_{1r}(x)dx \tag{A-29}$$

Superscript $p \times q$ is used to refer to rows $p$ and columns $q$. State-space matrices:

$$A_s = \begin{bmatrix} -2\zeta\omega_{s1} + f_{l\zeta} & \cdots & 0 & -\omega_{s1}^2 + f_{l\omega 1} & \cdots & 0 \\ \vdots & \ddots & \vdots & \vdots & \ddots & \vdots \\ 0 & \cdots & -2\zeta\omega_{sNs} + f_{l\zeta Ns} & 0 & \cdots & -\omega_{sNs}^2 + f_{l\omega Ns} \\ 1 & \cdots & 0 & 0 & \cdots & 0 \\ \vdots & \ddots & \vdots & \vdots & \ddots & \vdots \\ 0 & \cdots & 1 & 0 & \cdots & 0 \end{bmatrix} \tag{A-30}$$

$$B_s = \begin{bmatrix} W_{13}(L_3)/m_1 & -\theta\partial W_{11}(L1)/m_1 \\ \vdots & \vdots \\ W_{Ns3}(L_3)/m_{Ns} & -\theta\partial W_{Ns1}(L1)/m_{Ns} \\ 0 & 0 \end{bmatrix} \tag{A-31}$$

$$C_s = \begin{bmatrix} -W_{r3}(L_3)A_s^{1:Ns\times 2Ns} & \cdots \\ -W_{r3}(L_3) & 0 \\ 0 & W_{r3}(L_{laser}) \end{bmatrix} \tag{A-32}$$

$$D_s = \begin{bmatrix} W_{r3}(L_3)B_s^{1:Ns\times 2} & \cdots \\ 0 & 0 \\ 0 & 0 \end{bmatrix} \tag{A-33}$$

## State-space of the wing

Superscript $p \times q$ is used to refer to rows $p$ and columns $q$. Derive $A_w$ matrix by taking partial derivatives of the Euler equation (A-34) and the lag-states (A-35) to the system states:

$$E = \int_{-b}^{b} (\varepsilon - ab) m(\varepsilon) \ddot{\xi}(\varepsilon/b, t) d\varepsilon - M_L = 0 \tag{A-34}$$

$$\dot{z}_i = \frac{b_i A_i U}{b} Q(t) - \frac{b_i}{b} U z_i(t) \tag{A-35}$$

$$A_w = \begin{bmatrix} -\frac{\partial E}{\partial \dot{\alpha}} / \frac{\partial E}{\partial \ddot{\alpha}} & -\frac{\partial E}{\partial \alpha} / \frac{\partial E}{\partial \ddot{\alpha}} & -\frac{\partial E}{z_i} / \frac{\partial E}{\ddot{\alpha}} \\ 1 & 0 & 0 \\ \frac{\partial \dot{z}_i}{\partial \dot{\alpha}} & \frac{\partial \dot{z}_i}{\partial \alpha} & \frac{\partial \dot{z}_i}{\partial z_i} \end{bmatrix} \tag{A-36}$$

Take a comparable approach for determining the $B_w$, but the derivative to the inputs of the system:

$$B_w = \begin{bmatrix} -\frac{\partial E}{\partial \dot{h}} & -\frac{\partial E}{\partial \ddot{h}} \\ 0 & 0 \\ \frac{\partial \dot{z}_i}{\partial \dot{h}} & -\frac{\partial \dot{z}_i}{\partial \ddot{h}} \end{bmatrix} \tag{A-37}$$

Repeat the same procedure for the Newton equation results in the $C_w$ and $D_w$ matrix.

$$F_{wing} = \int_{-b}^{b} m(\varepsilon) \ddot{\xi}(\varepsilon, t) d\varepsilon - F_L \tag{A-38}$$

$$C_w = \begin{bmatrix} \frac{\partial F_{wing}}{\partial \dot{\alpha}} & \frac{\partial F_{wing}}{\partial \alpha} & \frac{\partial F_{wing}}{z_i} \end{bmatrix} \tag{A-39}$$

$$+ \frac{\partial F_{wing}}{\partial \ddot{\alpha}} A_w^{1 \times 4} \tag{A-40}$$

$$D_w = \begin{bmatrix} \frac{\partial F_{wing}}{\partial \ddot{h}} & \frac{\partial F_{wing}}{\partial \dot{h}} \end{bmatrix} \tag{A-41}$$

$$+ \frac{\partial F_{wing}}{\partial \ddot{\alpha}} B_w^{1 \times 2} \tag{A-42}$$

# Appendix B

# Theodorsen Theory

Aerodynamic forces on an airfoil are reduced as a result of the wake [23]. A very popular modal for the wake effect is derived by Theodorsen [21].

## Theodorsen approach for unsteady aerodynamics

Basis of Theodorsen's theory is formed by the Bernoulli equation, combined with the potential flow theory. Where the potential flows $\varphi$ determines the local flow velosities.The resulting local pressure is given by (B-2)[21]. Constants $\rho$ and $U$ are the air density and free stream velocity respectively. Coordinates of the airfoil are defined by ($\varepsilon$,$y$) and $\varepsilon = 0$ is ad the mid-chord. For a airfoil with semi-chord length $b$ the coordinate $\varepsilon = -b$ refers to the leading edge and $\varepsilon = b$ to the trailing edge. For the calculations the dimensionless coordinate $x$ is used, which is defined by a normalisation $x = \varepsilon/b$.

$$\Delta P(\varepsilon) = -2\rho\left(\frac{\partial\varphi}{\partial t}(\varepsilon) + U\frac{\partial\varphi}{\partial\varepsilon}(\varepsilon)\right) \tag{B-1}$$

$$\Delta P(x) = -2\rho\left(\frac{\partial\varphi}{\partial t}(x) + \frac{U}{b}\frac{\partial\varphi}{\partial x}(x)\right) \tag{B-2}$$

The potential flow can be divided into circular potential flow $\varphi_c$ and a non-circulatory part $\varphi_{nc}$. Where the non-circulatory part is a result of the flow around the airflow and the circulatory part is a result of the wake.

$$\varphi(x) = \varphi_{nc}(x) + \varphi_c(x)$$

### Non-circulatory flow

For the non circulatory part the potential flows are[21]:

$$\begin{aligned}
\varphi_{nc}(x) &= \varphi_{\alpha} + \varphi_{\dot{\alpha}} + \varphi_{h} + \varphi_{\dot{h}}(x) \\
\varphi_{\alpha}(x) &= bU\sqrt{1-x^2}\alpha(t) \\
\varphi_{\dot{\alpha}}(x) &= b^2(0.5x-a)\sqrt{1-x^2}\dot{\alpha}(t) \\
\varphi_{h}(x) &= 0 \\
\varphi_{\dot{h}}(x) &= b\sqrt{1-x^2}\dot{h}(t)
\end{aligned}$$

Substitution in the Bernoulli equation (B-2) results in the local pressure:

$$\begin{aligned}
\Delta P_{nc}(x) &= -2\rho_{air}\left(\frac{\partial \varphi_{nc}}{\partial t}(x) + \frac{U}{b}\frac{\partial \varphi_{nc}}{\partial x}(x)\right) \\
&= -2\rho_{air}b\sqrt{1-x^2}\left(U\dot{\alpha}(t) + b(0.5x-a)\ddot{\alpha}(t) + \ddot{h}(t)\right) \\
&\quad + 2\rho_{air}U\frac{x}{\sqrt{1-x^2}}\left(U\alpha(t) + b(0.5x-a)\dot{\alpha}(t) + \dot{h}(t)\right) \\
&\quad - \rho_{air}bU\sqrt{1-x^2}\dot{\alpha}(t)
\end{aligned}$$

Now the non-circulatory normal force $N_{nc}$ is obtained by integrating the local pressure over the entire airfoil:

$$\begin{aligned}
N_{nc} &= \int_0^s \int_{-b}^b \Delta P_{nc}(\varepsilon) d\varepsilon dy \\
&= sb\int_{-1}^1 \Delta P_{nc}(x) dx \\
&= -2\rho_{air}bs\int_{-1}^1 \frac{\partial \varphi_{nc}}{\partial t}(x) + \frac{Us}{b}\frac{\partial \varphi_{nc}}{\partial x}(x) dx \\
&= -2\rho_{air}b\int_{-1}^1 \frac{\partial \varphi_{nc}}{\partial t}(x) dx - \frac{2\rho_{air}U}{b}\varphi_{nc}(x)|_{-1}^1 \\
&= -\pi\rho_{air}sb^2\left(U\dot{\alpha}(t) - ab\ddot{\alpha} + \ddot{h}(t)\right)
\end{aligned}$$

For the moment around the pivot $\varepsilon = ab$ the local pressure needs to be multiplied by $(\varepsilon - ab)$.

Resulting in a

$$\begin{aligned}
M_{nc} &= \int_0^s \int_{-b}^{b} (\varepsilon - ab)\Delta P_{nc}(\varepsilon) d\varepsilon dy \\
&= sb^2 \int_{-1}^{1} (x-a)\Delta P_{nc}(x) dx \\
&= sb^2 \int_{-1}^{1} x\Delta P_{nc}(x) dx - sab^2 \int_{-1}^{1} \Delta P_{nc}(x) dx \\
&= -2\rho_{air} sb^2 \int_{-1}^{1} x \left( \frac{\partial \varphi}{\partial t}(x) + \frac{sU}{b} \frac{\partial \varphi}{\partial x}(x) \right) dx - sabN_{nc} \\
&= -2\rho_{air} sb^2 \int_{-1}^{1} x \frac{\partial \varphi}{\partial t}(x) dx + 2\rho_{air} sbU \int_{-1}^{1} \varphi_{nc}(x) dx - sabN_{nc} \\
&= \pi \rho_{air} sb^2 \left( U^2 \alpha(t) + U\dot{h}(t) - b^2 \left( 0.125 + a^2 \right) \ddot{\alpha} + ab\ddot{h}(t) \right)
\end{aligned}$$

## Circulatory flow

Assume for the circulatory flow that the vortex moves with free stream velocity. The normalised coordinate $x_0$ is used for the downstream vortex. With a constant velocity the the following statement holds [21]

$$\frac{\partial \varphi}{\partial t} = \frac{U}{b} \frac{\partial \varphi}{\partial x_0}$$

Resulting in the local pressure:

$$\Delta P_c(x, x_0) = -\frac{2\rho_{air} U}{b} \left( \frac{\partial \varphi}{\partial x} + \frac{\partial \varphi}{\partial x_0} \right)$$

The vortex $\Delta\Gamma$ is normalised and can be written as[23].

$$\Delta\Gamma = b\gamma dx_0$$

For the circulatory part the potential flow are[21]:

$$\varphi_\Gamma(x) = -\frac{\Delta\Gamma}{2\pi} \left( \frac{\sqrt{1-x^2}\sqrt{1-{x_0}^2}}{1-xx_0} \right) \varphi_\gamma(x) \quad = -\frac{b}{2\pi} \int_1^\infty \tan^{-1} \left( \frac{\sqrt{1-x^2}\sqrt{1-{x_0}^2}}{1-xx_0} \right) \gamma dx_0$$

The potential flow should satisfy the Kutta condition.

$$\lim_{x \to 1} \frac{\partial \varphi_{tot}}{\partial x}(x) < \infty$$

Where the partial derivatives of the potential flows are:

$$\begin{aligned}
\frac{\partial \varphi_{nc}}{\partial x}(x) &= \frac{b}{\sqrt{1-x^2}} \frac{1}{2\pi} \int_{-1}^{\infty} \frac{\sqrt{{x_0}^2 - 1}}{x_0 - x} \gamma dx_0 \\
\frac{\partial \varphi_c}{\partial x}(x) &= \frac{b}{\sqrt{1-x^2}} \left( -\left( U\alpha(t) + \dot{h}(t) + b\left(0.5x - a\right)\dot{\alpha}(t) \right) x + 0.5b(1-x^2)\dot{\alpha}(t) \right)
\end{aligned}$$

Substitution of $x = -1$:

$$\lim_{x \to 1} \frac{\partial \varphi_{nc}}{\partial x}(x) + \frac{\partial \varphi_c}{\partial x}(x) < \infty$$

In order to be finite the following equation should hold:

$$Q(t) = \frac{1}{2\pi} \int_{-1}^{\infty} \frac{\sqrt{x_0 + 1}}{\sqrt{x_0 - 1}} \gamma dx_0 \tag{B-3}$$

$$= \left( U\alpha(t) + \dot{h}(t) + b\,(0.5 - a)\,\dot{\alpha}(t) \right) \tag{B-4}$$

Now we define $C$ as:

$$C = \frac{\int_1^{\infty} \frac{x_0}{\sqrt{{x_0}^2 - 1}} \gamma dx_0}{\int_1^{\infty} \frac{\sqrt{x_0 + 1}}{\sqrt{x_0 - 1}} \gamma dx_0} \tag{B-5}$$

The complete expression for the local pressure:

$$\begin{aligned}
\Delta P_c(x, x_0) &= -\frac{\rho_{air} \Delta \Gamma U}{\pi b} \frac{x_0 + x}{\sqrt{1 - x^2}\sqrt{{x_0}^2 - 1}} \\
&= -\frac{\rho_{air} \Delta \Gamma U}{\pi b} \left( \frac{1}{\sqrt{1 - x^2}} \frac{x_0}{\sqrt{{x_0}^2 - 1}} + \frac{x}{\sqrt{1 - x^2}} \frac{1}{\sqrt{{x_0}^2 - 1}} \right) \\
&= -\frac{\rho_{air} \Delta \Gamma U}{\pi b} \left( \frac{1 - x}{\sqrt{1 - x^2}} \frac{x_0}{\sqrt{{x_0}^2 - 1}} + \frac{x}{\sqrt{1 - x^2}} \frac{\sqrt{x_0 + 1}}{\sqrt{x_0 - 1}} \right)
\end{aligned}$$

By the substitution of (B-3) and (B-5):

$$\begin{aligned}
\Delta P_c(x) &= -\frac{\rho_{air} U}{\pi} \left( \frac{1 - x}{\sqrt{1 - x^2}} \int_1^{\infty} \frac{x_0}{\sqrt{{x_0}^2 - 1}} \gamma dx_0 + \frac{x}{\sqrt{1 - x^2}} \int_1^{\infty} \frac{\sqrt{x_0 + 1}}{\sqrt{x_0 - 1}} \gamma dx_0 \right) \\
&= -2\rho_{air} U \left( \frac{1 - x}{\sqrt{1 - x^2}} C Q(t) + \frac{x}{\sqrt{1 - x^2}} Q(t) \right)
\end{aligned}$$

Similarly as before as before the normal force is derived by integrating:

$$\begin{aligned}
N_c &= \int_0^s \int_{-b}^b \Delta P_c(\varepsilon) d\varepsilon dy \\
&= sb \int_{-1}^1 \Delta P_c(x) dx \\
&= -2\pi \rho_{air} sbUCQ(t)
\end{aligned}$$

For the momentum first the multiplication with $(\varepsilon - ab)$:

$$\begin{aligned}
M_c &= \int_0^s \int_{-b}^b (\varepsilon - ab) \Delta P_c(\varepsilon) d\varepsilon dy \\
&= sb^2 \int_{-1}^1 (x - a) \Delta P_c(x) dx \\
&= 2\pi \rho_{air} sb^2 U (0.5 + a) C Q(t) - \pi \rho_{air} sb^2 U Q(t)
\end{aligned}$$

### Total force and moment

Simply ad non-circulatory and circulatory forces:

$$\begin{aligned} F_L &= N_{nc} + N_c \\ &= -\pi\rho_{air} s b^2 \left( U\dot{\alpha}(t) - ab\ddot{\alpha} + \ddot{h}(t) \right) \\ &\quad - 2\pi\rho_{air} s b U C Q(t) \end{aligned}$$

Same for momentum:

$$\begin{aligned} M_L &= M_{nc} + M_c \\ &= \pi\rho_{air} s b^2 \left( U^2\alpha(t) + U\dot{h}(t) - b^2\left(0.125 + a^2\right)\ddot{\alpha}(t) + ab\ddot{h}(t) \right) \\ &\quad + 2\pi\rho_{air} s b^2 U(0.5 + a) C Q(t) - \pi\rho_{air} s b^2 U Q(t) \end{aligned}$$

Which can be simplified by the substitution of (B-4).

$$\begin{aligned} M_L = \pi\rho_{air} s b^2 &\left( -bU\left(0.5 - a\right)\dot{\alpha}(t) - b^2\left(0.125 + a^2\right)\ddot{\alpha}(t) + ab\ddot{h}(t) \right) \\ &+ 2\pi\rho_{air} s b^2 U(0.5 + a) C Q(t) \end{aligned}$$

# Appendix C

# Matlab code

## C-1 Spectral analysis with frequency averaging

Written by Ivo Houtzager from the Delft Center of Systems and Control (2008):

```
function [G,w,Coh,mSuu,mSyy] = spa_avf(u,y,r,dt,Nband,Nfft,ZeroPadding,
    Wname)
%SPA_AVF Spectral analysis with frequency averaging
%   [G,W]=SPA_AVF(U,Y,Ts,Nband) determines a frequency domain estimate
%   SYS=FRD(G,W) of the transfer function of the plant. The sample time
    is
%   given in Ts. Nband is the number of frequency bands to average.
%   Averaging in the frequency domain is used to get a smoother frequency
%   response function. The spectrum is smoothed locally in the region of
%   the target frequencies, as a weighted average of values to the right
%   and left of a target frequency. The variance of the spectrum will
%   decrease as the number of frequencies used in the smoothing increases
    .
%   As the bandwidth increases, more spectral ordinates are averaged, and
%   hence the resulting estimator becomes smoother, more stable and has
%   smaller variance.

%   [G,W]=SPA_AVF(U,Y,R,Ts,Nband) determines a frequency domain estimate
%   SYS=FRD(G,W) of the transfer function of the plant operating in
%   closed loop. Because the conventional transfer function estimate,
    will
%   give a biased estimate under closed loop [2]. An unbiased alternative
%   is to use cross spectral between the input/output signals with an
%   external excitation signal r [1]. Hence, we define the estimate:
%            G(exp(j*omega)) = Phi_yr(omega)*inv(Phi_ur(omega))

%   [G,W]=SPA_AVF(...,Ts,Nband,Nfft) specifies the number of evaluated
%   frequencies. For large data sequences it is wortwhile to choose the
%   value Nfft as function of the power of two. In this case a faster
```

```
26 %   method is used durring the FFT. Nfft <= length(u), unless zeros are
27 %   added. See also, FFT.
28
29 %   [G,W]=SPA_AVF(...,Ts,Nband,Nfft,ZeroPading) adds additional zeros to
30 %   the data sequences. Usefull for increasing the number of evaluated
31 %   frequencies.
32
33 %   [G,W]=SPA_AVF(...,Ts,Nband,Nfft,ZeroPading,Wname) specifies and
   aplies
34 %   an window to the data. Windowing weigths the data, it increases the
35 %   importance of the data in the middle of the vector and decreases the
36 %   importance of the data at the end and the beginning, thus reducing
   the
37 %   effect of spectral leakage. See also, WINDOW.
38
39 %   Revsion 2: Now also works properly for MIMO cases.
40
41 % References:
42 %   [1] Akaike, H., Some problems in the application of the cross
   spectral
43 %       method, In spectral analysis of time series, pp. 81 107, Wiley,
44 %       New York, 1967.
45 %   [2] van den Hof, P., System Identification, Lecture Notes, Delft,
   2007.
46
47 %  Ivo Houtzager
48 %
49 %  Delft Center of Systems and Control
50 %  The Netherlands, 2008
51
52 % Check closed loop
53 if isequal(length(u),length(r));
54     clmode = 1;
55 else
56     clmode = 0;
57     if nargin == 7
58         Wname = ZeroPadding;
59     end
60     if nargin == 6
61         ZeroPadding = Nfft;
62     end
63     if nargin == 5
64         Nfft = Nband;
65     end
66     Nband = dt;
67     dt = r;
68 end
69
70 % Transpose vectors if needed
71 if size(u,2) < size(u,1);
72     u = u';
73 end
74 nu = size(u,1); % number of inputs
```

```
75  if size(y,2) < size(y,1);
76      y = y';
77  end
78  ny = size(y,1); % number of inputs
79  if clmode
80      if size(r,2) < size(r,1);
81          r = r';
82      end
83      nr = size(r,1); % number of inputs
84  end
85
86  % Apply window and zeros if needed
87  if nargin == (7+clmode)
88      u = u.*(ones(nu,1)*window(Wname,size(u,2))');
89      y = y.*(ones(ny,1)*window(Wname,size(u,2))');
90      if clmode
91          r = r.*(ones(nr,1)*window(Wname,length(u))');
92      end
93  end
94  if nargin == (6+clmode)
95      u = [u zeros(nu,ZeroPadding)];
96      y = [y zeros(ny,ZeroPadding)];
97      if clmode
98          r = [r zeros(nr,ZeroPadding)];
99      end
100 end
101 if nargin < (5+clmode)
102     Nfft = [];
103 end
104
105 % Some administration
106 Fs = 1./dt;                          % Sample frequency
107 N  = length(u);                      % Number of samples
108 T  = N*dt;                           % Total time
109 if isempty(Nfft)
110     f = (0:N1)'/T;                   % Frequency vector (double sided)
111 else
112     f = (linspace(0,N1,Nfft))'/T;    % Frequency vector (double sided)
113 end
114 Nf = length(f);
115
116 % Determine Fourier transforms
117 U = zeros(nu,1,Nf);
118 Y = zeros(ny,1,Nf);
119 for i = 1:nu
120     ut = dt*fft(u(i,:),Nfft);
121     for k = 1:Nf
122         U(i,:,k) = ut(k);
123     end
124 end
125 for i = 1:ny
126     yt = dt*fft(y(i,:),Nfft);
127     for k = 1:Nf
```

```
128             Y(i,:,k) = yt(k);
129         end
130     end
131     if clmode
132         R = zeros(nu,1,Nf);
133         for i = 1:nr
134             rt = dt*fft(r(i,:),Nfft);
135             for k = 1:Nf
136                 R(i,:,k) = rt(k);
137             end
138         end
139     end
140
141     % Do closed loop or open loop
142     if clmode
143         % Determine spectral densities
144         Sur = zeros(nu,nr,Nf);
145         Suu = zeros(nu,nu,Nf);
146         Srr = zeros(nr,nr,Nf);
147         Syr = zeros(ny,nr,Nf);
148         Syy = zeros(ny,ny,Nf);
149         for k = 1:Nf
150             Suu(:,:,k) = (1/T).*U(:,:,k)*U(:,:,k)';
151             Sur(:,:,k) = (1/T).*U(:,:,k)*R(:,:,k)';
152             Srr(:,:,k) = (1/T).*R(:,:,k)*R(:,:,k)';
153             Syr(:,:,k) = (1/T).*Y(:,:,k)*R(:,:,k)';
154             Syy(:,:,k) = (1/T).*Y(:,:,k)*Y(:,:,k)';
155         end
156
157         % Apply frequency averaging
158         Nmod = floor(Nf/Nband);
159         mSuu = zeros(nu,nu,Nmod);
160         mSur = zeros(nu,nr,Nmod);
161         mSrr = zeros(nr,nr,Nmod);
162         mSyr = zeros(ny,nr,Nmod);
163         mSyy = zeros(ny,ny,Nmod);
164         mf = freqAvg(f,Nband);
165         for i = 1:nr
166             for j = 1:nr
167                 tSur = Sur(i,j,:);
168                 tSur = freqAvg(tSur(:),Nband);
169                 mSur(i,j,:) = tSur;
170                     tSuu = Suu(i,j,:);
171                 tSuu = freqAvg(tSuu(:),Nband);
172                 mSuu(i,j,:) = tSuu;
173
174                 tSrr = Srr(i,j,:);
175                 tSrr = freqAvg(tSrr(:),Nband);
176                 mSrr(i,j,:) = tSrr;
177             end
178         end
179         for i = 1:ny
180             for j = 1:ny
```

```
181             tSyy = Syy(i,j,:);
182             tSyy = freqAvg(tSyy(:),Nband);
183             mSyy(i,j,:) = tSyy;
184         end
185         for j = 1:nr
186             tSyr = Syr(i,j,:);
187             tSyr = freqAvg(tSyr(:),Nband);
188             mSyr(i,j,:) = tSyr;
189         end
190     end
191
192     % Estimate transfer function
193     G = zeros(ny,nr,Nmod);
194     for k = 1:Nmod
195         G(:,:,k) = mSyr(:,:,k)/mSur(:,:,k);
196     end
197
198     % Squared coherence Cohuy function between r and y
199     if nr == ny && nargout == 3
200         Coh = zeros(ny,nr,Nmod);
201         for k = 1:Nmod
202             Coh(:,:,k) = sqrtm(abs(mSyr(:,:,k))*abs(mSyr(:,:,k))/(mSyy
                    (:,:,k)*mSrr(:,:,k)));
203         end
204     end
205 else
206     % Determine spectral densities
207     Suu = zeros(nu,nu,Nf);
208     Syu = zeros(ny,nu,Nf);
209     Syy = zeros(ny,ny,Nf);
210     for k = 1:Nf
211         Suu(:,:,k) = (1/T).*U(:,:,k)*U(:,:,k)';
212         Syu(:,:,k) = (1/T).*Y(:,:,k)*U(:,:,k)';
213         Syy(:,:,k) = (1/T).*Y(:,:,k)*Y(:,:,k)';
214     end
215
216     % Apply frequency averaging
217     Nmod = floor(Nf/Nband);
218     mSuu = zeros(nu,nu,Nmod);
219     mSyu = zeros(ny,nu,Nmod);
220     mSyy = zeros(ny,ny,Nmod);
221     mf = freqAvg(f,Nband);
222     for i = 1:nu
223         for j = 1:nu
224             tSuu = Suu(i,j,:);
225             tSuu = freqAvg(tSuu(:),Nband);
226             mSuu(i,j,:) = tSuu;
227         end
228     end
229     for i = 1:ny
230         for j = 1:ny
231             tSyy = Syy(i,j,:);
232             tSyy = freqAvg(tSyy(:),Nband);
```

```
233             mSyy(i,j,:) = tSyy;
234         end
235         for j = 1:nu
236             tSyu = Syu(i,j,:);
237             tSyu = freqAvg(tSyu(:),Nband);
238             mSyu(i,j,:) = tSyu;
239         end
240     end
241
242     % Estimate transfer function
243     G = zeros(ny,nu,Nmod);
244     for k = 1:Nmod
245         G(:,:,k) = mSyu(:,:,k)/mSuu(:,:,k);
246     end
247
248     % Squared coherence Cohuy function between u and y
249     if nu == ny && nargout> 2
250         Coh = zeros(ny,nu,Nmod);
251         for k = 1:Nmod
252             Coh(:,:,k) = sqrtm(abs(mSyu(:,:,k))*abs(mSyu(:,:,k))/(mSyy
                    (:,:,k)*mSuu(:,:,k)));
253         end
254     end
255 end
256
257 % Construct function output
258 fmax = Fs/2;
259 fi = find(mf <= fmax);
260 w = mf(fi).*2*pi;
261 G = G(:,:,fi);
262 mSuu=mSuu(:,:,fi);
263 mSyy=mSyy(:,:,fi);
264 %Coh=[];
265 if nu == ny && nargout > 2
266     Coh = Coh(:,:,fi);
267 end
268 end
269
270 function out = freqAvg(in,nrbands)
271 %FREQAVG Frequency averaging
272 %  out=freqAvg(in,nrbands) averages the input 'in' over the number of
273 %  frequency bands 'nrbands'.
274
275 N       = length(in);
276 Nmod    = floor((N/nrbands));   % number of remaining frequencies after
    averaging
277 tmp     = zeros(nrbands,Nmod);  % initialization of temporary matrix for
    averaging: nrband rows and nmod columns
278 tmp(:) = in(1:nrbands*Nmod);    % arrange the samples of 'in' in the
    elements of tmp.
279 out     = mean(tmp,1)';         % average over columns and make it a
    vector
280 end
```

# Bibliography


[1] BP, "Bp statistical review of world energy 2015," 2015.

[2] E. C. Renewable energy progress report Brussels, 15.6.2015.

[3] P. Moriarty and D. Honnery, "Can renewable energy power the future?," *Energy Policy*, vol. 93, pp. 3–7, 2016.

[4] M. Z. Jacobson and M. A. Delucchi, "Providing all global energy with wind, water, and solar power, part i: Technologies, energy resources, quantities and areas of infrastructure, and materials," *Energy Policy*, vol. 39, no. 3, pp. 1154–1169, 2011.

[5] M. M. Bernitsas, K. Raghavan, Y. Ben-Simon, and E. Garcia, "Vivace (vortex induced vibration aquatic clean energy): A new concept in generation of clean and renewable energy from fluid flow," *Journal of Offshore Mechanics and Arctic Engineering*, vol. 130, no. 4, p. 041101, 2008.

[6] J. McCarthy, S. Watkins, A. Deivasigamani, and S. John, "Fluttering energy harvesters in the wind: A review," *Journal of Sound and Vibration*, vol. 361, pp. 355–377, 2016.

[7] M. Bryant, A. D. Schlichting, and E. Garcia, "Toward efficient aeroelastic energy harvesting: device performance comparisons and improvements through synchronized switching," in *SPIE Smart Structures and Materials+ Nondestructive Evaluation and Health Monitoring*, pp. 868807–868807, International Society for Optics and Photonics, 2013.

[8] E. Naudascher and D. Rockwell, *Flow-induced vibrations: an engineering guide*. Courier Corporation, 2012.

[9] H.-J. Jung and S.-W. Lee, "The experimental validation of a new energy harvesting system based on the wake galloping phenomenon," *Smart Materials and Structures*, vol. 20, no. 5, p. 055022, 2011.

[10] M. Bryant, R. L. Mahtani, and E. Garcia, "Wake synergies enhance performance in aeroelastic vibration energy harvesting," *Journal of Intelligent Material Systems and Structures*, vol. 23, no. 10, pp. 1131–1141, 2012.

[11] M. Bryant, E. Wolff, and E. Garcia, "Parametric design study of an aeroelastic flutter energy harvester," in *SPIE Smart Structures and Materials+ Nondestructive Evaluation and Health Monitoring*, pp. 79770S–79770S, International Society for Optics and Photonics, 2011.

[12] M. Bryant, A. D. Schlichting, and E. Garcia, "Toward efficient aeroelastic energy harvesting: device performance comparisons and improvements through synchronized switching," in *SPIE Smart Structures and Materials+ Nondestructive Evaluation and Health Monitoring*, pp. 868807–868807, International Society for Optics and Photonics, 2013.

[13] L. Zhao and Y. Yang, "Enhanced aeroelastic energy harvesting with a beam stiffener," *Smart Materials and Structures*, vol. 24, no. 3, p. 032001, 2015.

[14] B. Huynh, T. Tjahjowidodo, Z. Zhong, Y. Wang, and N. Srikanth, "Nonlinearly enhanced vortex induced vibrations for energy harvesting," in *Advanced Intelligent Mechatronics (AIM), 2015 IEEE International Conference on*, pp. 91–96, IEEE, 2015.

[15] A. Erturk and D. J. Inman, "A distributed parameter electromechanical model for cantilevered piezoelectric energy harvesters," *Journal of vibration and acoustics*, vol. 130, no. 4, p. 041002, 2008.

[16] M. Bryant and E. Garcia, "Modeling and testing of a novel aeroelastic flutter energy harvester," *Journal of vibration and acoustics*, vol. 133, no. 1, p. 011010, 2011.

[17] M. Gaunaa, "Unsteady 2d potential-flow forces on a thin variable geometry airfoil undergoing arbitrary motion," tech. rep., 2006.

[18] S. R. Moheimani and A. J. Fleming, *Piezoelectric transducers for vibration control and damping*. Springer Science & Business Media, 2006.

[19] S. S. Rao and F. F. Yap, *Mechanical vibrations*. Pearson Education South Asia, 2011.

[20] P. A. Lagace, "Unit 23: Vibration of continuous systems," *MIT - lecture slides "http://ocw.mit.edu/courses/aeronautics-and-astronautics/16-20-structural-mechanics-fall-2002/lecture-notes/unit23.pdf" [07-11-2016]*, 2001.

[21] T. Theodorsen, "General theory of aerodynamic instability and the mechanism of flutter," 1949.

[22] T. Buhl, M. Gaunaa, and C. Bak, "Potential load reduction using airfoils with variable trailing edge geometry," *Journal of Solar Energy Engineering*, vol. 127, no. 4, pp. 503–516, 2005.

[23] G. Dimitriadis, "Lecture 6: Unsteady aerodynamics - theodorsen," *ULg (Université de Liege - lecture slides)"http://www.ltas-aea.ulg.ac.be/cms/uploads/Aeroelasticity06.pdf" [01-01-2017]*.

# Glossary

## List of Acronyms

| | |
|---|---|
| **DCSC** | Delft Center for Systems and Control |
| **EIE** | Extraneously Induced Excitation, by fluctuations in the fluid flow |
| **IIE** | Instability Induced Excitation, by fluctuations induced by the structure |
| **MIE** | Movement Induced Excitation, by the movement of the structure |
| **MFC** | Macro Fiber Composite, is a piezoelectric material |
| **ADC** | Analog to Digital Converter |
| **DAC** | Digital to Analog Conversion |
| **VAF** | Variance Accounted For |

## List of Symbols

### Greek Symbols

| | |
|---|---|
| $\varphi_c$ | Circular velocity field |